NASA-CR-196109

IN-33-CR
I.C.T.
14047
60P

FINAL TECHNICAL REPORT

for

Cooperative Agreement NCC 3-55

with

NASA - Lewis Research Center

Theoretical Studies of the Transport Properties in Compound Semiconductors

Principal Investigator: Benjamin Segall

Department of Physics
Case Western Reserve University

(NASA-CR-196109) THEORETICAL STUDIES OF THE TRANSPORT PROPERTIES IN COMPOUND SEMICONDUCTORS Final Technical Report (Case Western Reserve Univ.) 60 p

N94-37501

Unclas

G3/33 0014047

INTRODUCTION

This final report is an overview of the work done on Cooperative Agreement NCC 3-55 with the Solid State Technology Branch of the NASA-Lewis Research Center (LeRC). Over the period of time that the agreement was in effect, the principal investigator - and in the last three year - the co-principal investigator (Walter R. Lambrecht) worked on a significant number of projects and interacted with members of the Solid State Technology (SST) branch in a number of different ways. For the purpose of this report, these efforts will be divided into five categories: 1) work directly with experimental electrical transport studies conducted by members of the SST branch; 2) theoretical work on electrical transport in compound semiconductors; 3) electronic structure calculations which are relevant to the electrical transport in polytypes of SiC and SiC-AlN alloys; 4) the electronic structure calculations of polar interfaces; and 5) consultative and supportive activities related to experiments and other studies carried out by SST branch members. Work in these categories will be briefly discussed below. Much of the past work was discussed in more detail in the various proposals for this grant.

Copies of references [4], [5], [6] and [7] are attached to this report. Copies of references [1], [2] and [3], which also acknowledge support by this grant, are not included as the monitor of this grant is a co-author of those publications and thus has copies of them.

WORK CARRIED OUT UNDER THE AGREEMENT

(1). Work Directly Connected with Experimental Electrical Transport Studies Conducted by Members of the SST branch:

Because of SiC potentialities in a wide range of applications, in particular, semiconductor applications at high temperature, high fields and high frequencies, this material has attracted considerable interest over the last decade. In the early 1980s, researchers at LeRC were the first to grow epitaxially large area crystal films. This was done by the chemical vapor deposition (CVD) method. Thus, there was considerable interest at LeRC to determine the electrical transport properties of those films. We note here that while SiC can form in a large number of crystallographic structures (polytypes), those films had the 3C (the cubic) structure. The electrical properties are obtained by so-called Hall measurements. A series of such measurements on several films produced at LeRC was initiated by Drs. E. J. Haugland and S. A. Alterovitz of the SST branch. The PI worked with these researchers to interpret the data in terms of the band structure of 3C SiC. The results of these investigations appeared in *Applied Physics Letters* [1].

About the time of this work, two other groups of researchers published the results of measurements on similar SiC films. Their analysis lead to different interpretations than ours. Our analysis of their results,which was also published [2], backed our interpretation, which is now the widely accepted interpretation.

Another project in this category was also related to experimental work by Drs. Haugland and Alterovitz along with that of a visiting researcher, Dr. P. P. Szydlik. This involved the study of the properties of the two-dimensional electron gas in a $In_{0.1}Ga_{0.9}$ As/GaAs heterostructure. In this structure the electrons reside in the InGaAs alloy, which has a smaller band gap than the GaAs. The experiments consisted of Hall and Shubnikov de Haas (SdH) measurements. The latter involves oscillations in the magnetoresistance. From analyses of the SdH oscillations as a function of temperature and as a function of magnetic field, it is possible to determine an effective mass m* and an electron scattering time τ_{SdH}. From the Hall mobility - determined in the Hall measurements - another electron scattering τ_H could be determined. It was found that the ratio τ_H / τ_{SdH} was about 5 to 6. The fact that the ratio was considerably larger than one was explained by the fact that while small angle scattering does not contribute appreciably to τ_H, it does contribute to τ_{SdH}. Relevant scattering mechanisms which could contribute to the difference were identified and the value of m* was discussed in terms of known values for the pure compounds. A paper on this work was published [3].

(2). Theoretical Work on Transport in Compound Semiconductors:

The aim of this work was to set up a reliable means for calculating the transport properties, in particular, the Hall mobility and the so-called Hall coefficient $r_H(T)$ (which is given by $R_H = r_H/en$ where R_H is the Hall constant and n(T) is electron

density). Both quantities, especially μ_H, depend on the various scattering mechanisms that are operative and on the nature of the electronic energies in the vicinity of the relevant band extremum, e.g., conduction band minimum (or minima). For SiC, and other semiconductors of current interest, both the mechanisms and the details of the band edges are not known with accuracy and certainty. The goal is to compare the calculated $\mu_H(T)$ with suitable experimental results over a reasonable range of T and thereby pin down the relevant scattering mechanisms and certain aspects of the band edges.

The PI, with the help of two CWRU undergraduate physics students, has set up programs to numerically solve the Boltzmann transport equations. All the principal scattering mechanisms relevant for compound semiconductors are included. The programs have been checked extensively. Of most immediate interest to us is the high temperature mobility of 3C SiC. Subsequent to that will be the study of the mobilities in the other polytypes; that will probably be a somewhat more involved undertaking.

(3). Electronic Structure Calculations Relevant to Electronic Transport in Polytypes of SiC and Related Materials:

A knowledge of the band structure is important for the transport because transport is effected by the nature of the band edge: whether it is degenerate or nondegenerate, whether it is at the center of the Brilloun Zone (BZ) and hence is a

single extremum, or is at some other $\vec{k}$ value in the BZ and hence is a "multi-vallied" extremum. In addition to having a large density of states, a multi-vallied band edge introduces the possibility of "intervalley scattering". Also important is the particular location of the extremum and the effective mass of the band edge.

The study of the band structure(s) of SiC is a significant project because, as noted earlier, SiC forms in numerous different structures, or polytypes. The different structures can be described by different orderings of the close-packed layers of atoms, these layers being the (111) plane of the cubic or the (0001) planes of the various hexagonal or rhombohedral structures. For our present purposes the 3C, 2H, 4H and 6H polytypes are the most important. The latter two are the most common and easily grown forms of SiC while the 2H (wurtzite) form is difficult to grow. The various structures differ in the frequency and ordering of the "cubic" and "hexagonal" stackings of the successive layers. With 3C having all the cubic and 2H all the hexagonal stacking, the sequence of the four polytypes in terms of increasing "hexagonality" is 3C, 6H, 4H and 2H.

Since the position of the valence band maximum of all the binary compound semiconductors, with the exception of AlN, are at $\vec{k}$=0, it is the conduction band minima which are of most concern. (All the values of the parameters describing the degenerate valence band maxima are unknown and thus, are of interest.) We first studied the 3C and 2H, the simplest forms of SiC. In all of our self-consistent calculations, we obtain the "energetic" properties (lattice constants, bulk moduli, and

cohesive energies) in addition to the band structure. It was found that the band gaps were indirect in both structures with the minimum for 3C being at the point X (of the fcc BZ) and that for 2H being at point K of the hexagonal BZ with a state at M being close in energy. We note that the points K and M are not the hexagonal equivalents of the point X when 2 BZs are appropriately superimposed. In addition to the "shifting" of the position of the conduction band edge, the band gap for 2H was found to be almost 1 eV larger than for 3C. To obtain a qualitative understanding of the above results, calculations for the closely related compound semiconductors AlN and GaN were carried out. An understanding was achieved and was described in a publication [4] acknowledging this grant.

More recent work included calculations of the 4H and 6H polytypes. With the results of these studies, we were able to determine the trends in the various band gaps including the minimum gaps of the aforementioned four polytypes as a function of hexagonality. This among other things was addressed in a publication [5] acknowledging the grant.

Further work studying the details of the conduction band edges is in progress. We note that recent transport studies conducted at the CREE Corporation have shown that the mobility of 4H SiC is higher and much more isotropic than that for the 6H form. These results can have significant implications for device applications, and represent one "hottest" unsettled issue in the SiC community. Tentative results from

our calculations may have some bearing on this question and will be pursued vigorously in the near future.

Finally, we note the work on alloys of SiC and the closely related compound AlN which is closely latticed matched to SiC. These alloys are of interest because AlN has a significantly larger band gap than SiC (for wurtzite AlN, E_g = 6.3 eV) so that the alloys will allow us to "tailor" the band gap over a large range. Moreover, for the equilibrium (wurtzite) form, AlN is direct. Thus, there is a crossover from an indirect to a direct band gap. A direct gap is advantageous for optical emission. Work on these alloys was briefly discussed in a report to the 1994 International Conference on SiC [6]. A more complete report will be written shortly.

(4). Electronic Structure Calculations of Polar Interfaces

Since semiconductor heterojunctions are now playing an important role in electronic technology and in basic physics, the study of the electronic structure at interfaces between semiconductors hardly needs justification. Such studies are generally done using the supercell approach, i.e., by studying a periodic superlattice of the two constituent semiconductors with a suitable (generally large) unit cell. However, when the interfaces are charged (the condition which characterizes "polar" interfaces), the calculated interfacial energy is the sum of the energies of the two oppositely charged interfaces. Since two interfaces are inequivalent, it is not possible to obtain the energies associated with the individual interfaces. Similarly, because of

the existence of an electrical field associated with the interfacial charges, it is also not possible to separate out the band offsets at the two interfaces. A scheme for circumventing this problem was worked out and published [7]. The approach was applied to polar inversion domain boundaries in GaAs and NaCl.

(5). Consultative and Supportive Activities

The PI has consulted with several members of the SST branch in connection with some of their projects. We briefly discusses a number of interactions.

The most frequent interactions were those with Dr. E. J. Haugland. The PI had numerous discussions with him about anticipated transport studies particularly those for SiC at relatively high temperatures. There were also numerous discussions with Dr. Haugland about his recent Hall data on 4H and 6H films.

The PI has, over the past several years, sought to obtain samples of 3C SiC of reasonably good quality for Dr. Haugland to study in the high temperature Hall apparatus that he has set up. Recently, we have finally succeeded in obtaining such samples from a research group in the Naval Research Laboratory. Hopefully, this will allow a definitive determination of the high temperature mobility of the cubic form. This will be compared with our theoretical calculations.

There were also discussions with Dr. Haugland about the interpretation of his electrical transport measurements of a number of GaAs crystals grown in space (on the STS-40 flight, June 1994). The properties of these samples differed from those of

earth-grown samples, which were otherwise as similar as possible to their space-grown counterparts. Dr. Haugland has reported on the data and on the (tentative) interpretation of them in internal NASA meetings

The PI also consulted with Rafael Mena on the changes in the electrical transport properties of the two-dimensional electron gas at the interface of AlGaAs/InGaAs heterojunctions produced by illumination. Among other issues, the effect of electron occupancy of the second and possibly higher subbands was discussed.

Finally, there were several discussions with Dr. David Rosenfeld on some transport problems in SiGe alloys in certain transistors.

REFERENCES

Articles Published Under the Grant

1. B. Segall, S. A. Alterovitz, E. J. Haugland and L. G. Matus, Appl. Phys. Lett., 49, 584, (1986).

2. B. Segall, S. A. Alterovitz, E. J. Haugland and L. G. Matus, Appl. Phys. Lett., 50, 1533, (1987).

3. P. P. Szydlik, S. A. Alterovitz, E. J. Haugland, B. Segall, T. S. Henderson, J. Klem and H. Morkoc, Superlattices and Microstructures, 4, 619, (1988).

4. W. R. Lambrecht and B. Segall, Mat. Res. Soc. Symp. Proc. Vol. 242, p367; 1992 Materials Research Society.

5. W. R. Lambrecht, C. H. Lee, K. Klein, A. E. Petukhov, E. A. Albanesi and B. Segall, Proc. NATO Advanced Workshop on Wide Band Gap Electronic Materials, Mensk, Belarus, May 4-6, 1994. To be published.

6. W. R. Lambrecht, E. A. Albanesi and B. Segall, Proc. International Conference on Silicon Carbide and Related Materials, Washington, DC, November 1993, Inst. of Phys. Publ., Ltd., Bristol, UK. Accepted for publication.

7. W. R. Lambrecht, C. Amador and B. Segall, Mat. Res. Soc. Symp. Proc. Vol. 253, p381; 1992 Materials Research Society.

A COMPARISON OF THE WURTZITE AND ZINCBLENDE BAND STRUCTURES FOR SiC, AlN AND GaN

W. R. L. LAMBRECHT and B. SEGALL
Department of Physics, Case Western Reserve University, Cleveland, OH 44106-7079

ABSTRACT

Total energy and band structure results of linear-muffin-tin orbital calculations within the atomic-sphere-approximation are presented for SiC, GaN and AlN in the zincblende and the wurtzite structure. We discuss the origin of the directness or indirectness and the relative magnitudes of the band gaps.

INTRODUCTION

In order to develop applications based on the electronic and optical properties of the promising wide band-gap semiconductors SiC, GaN and AlN, a thorough knowledge of their bulk band-structures and equilibrium properties is required. While some of this information is already available, it appears that there has not yet been a systematic study of the band-structures of this class of materials using the same approach. Such a study, which has the advantage that a *uniformly accurate* comparison between the various materials and structures can be made, is presented here.

An important aspect of these materials is the polymorphism. While SiC has a large number of polytypes, the nitrides GaN and AlN occur naturally only in the wurtzite (WZ) structure. They may, however, be stabilized in the zincblende (ZB) structure by epitaxial growth. While this possibility has already been demonstrated for GaN [1], it is still a challenge for AlN. The only report of ZB AlN refers to AlN precipitates formed inside an fcc Al matrix by N-ion implantation [2], obviously a non-equilibrium situation.

For optical applications, the question whether the bandgap is direct or indirect is very important. We will thus pay special attention to this issue.

COMPUTATIONAL METHOD

The underlying computational framework used in this work is the density functional theory [3] in the local density approximation (LDA). The linear muffin-tin orbital (LMTO) method [5] is used in the atomic sphere approximation (ASA) with the so-called combined correction.

In order to apply this approach to open structures such as ZB and WZ, so-called empty spheres must be introduced in order to appropriately describe the charge density and wave functions in the interstitial region. In the ZB case, the empty spheres are positioned at the tetrahedral interstitial sites. Equal sphere radii are used on all spheres in order to reduce the overlap between the spheres as much as possible. For the WZ structure, we introduced small empty spheres of radius $s_{E_1} \sim \frac{1}{4}s_A$ (s_A being the atomic sphere radius) in between the atoms along the c-direction and large empty spheres of size $s_{E_2} \sim 1.16 s_A$ in the channel regions. The Brillouin zone summations were converged to < 1 meV accuracy in the total energy results.

RESULTS

Equations of state

In this section, we present our results for the energy as a function of volume, i.e. the equations of state. We used a fit of the calculated results to the Rose-Smith-Ferrante equation of state [6] in order to extract the equilibrium volume/molecule, V; the cohesive energy, E_c; the bulk modulus, B; and the pressure derivative, B', of the latter. Table I summarizes the results.

ORIGINAL PAGE IS OF POOR QUALITY

Ref. 4

NLS

Table I: Equilibrium properties of SiC, AlN, GaN.

		V/molecule($Å^3$)	E_c(eV/molecule)	B(MBar)	B'
SiC	ZB	20.2 (20.7[a])	14.1 (12.7[b])	2.3 (2.2[c])	3.8
	WZ	19.9 (20.7[a])	14.6	2.4	3.9
AlN	ZB	20.3	12.6	2.2	3.9
	WZ	20.1 (20.8[a])	13.1 (11.5[b,a])	2.2 (2.1[d])	3.9
GaN	ZB	22.8	9.9	2.0	4.4
	WZ	21.7 (22.6[a])	10.2 (8.9[b])	2.2 (1.9[e])	4.1

Experimental values in parentheses.
a. Wyckoff [7]
b. From enthalpies of formation given in CRC Handbook [8]
c. Carnahan, [9]
d. Wettling and Windscheif [10]
e. Gerlich et al. [11]

The overall agreement with the experimental values (given in parentheses) is satisfactory. We note that our calculations may slightly overestimate the bulk modulus in the WZ structure because we did not minimize the energy with respect to the c/a ratio and internal degree of freedom u. We did not attempt this since it is well known from work on phonon-distortions in Si [12] that the ASA is not sufficiently accurate for studying the *effects of small structural* relaxations. The required accuracy can, however, be achieved by means of the full-potential (FP) *version* [12] of the LMTO-method. We recently carried out FP calculations of cubic SiC in order to determine its elastic constants [13]. Similar work on the nitrides and on the WZ structures is in progress. The above calculations predict the WZ structure to be stable with respect to the ZB in all cases by about 0.2-0.3 eV/atom. Cheng et al.'s work [14], however, indicates that for SiC, the ZB structure is lower in energy than the WZ by ~ 5 meV/atom. For GaN, Munoz and Kune [15] using pseudopotential calculations have recently found WZ to be stable with respect to ZB by only 15 meV/atom. To pin down these small structural energy differences, it appears to be essential to go beyond the ASA.

Band structures

To facilitate the *comparison* between the band structures in the ZB and the WZ structures, we follow the approach of Salehpour and Satpathy [16]. The ZB band structures are thus displayed in a double unit cell along axes in reciprocal space which are relevant for the hexagonal system. We refer to Ref. [16] for a complete discussion of the relationships between the k-points in the *two crystal structures*. In particular, we note that the point X_{fcc} of ZB lies at 2/3 of the way between the M and L points of the hexagonal Brillouin zone if the c/a ratio is ideal and is here indicated as X. The symmetry labels of the ZB band structures indicated in the Figs. 1-3 are those for the fcc Brillouin zone. The minimum bandgaps are given in Table II.

The *overall* features of the band structures agree well with previous calculations for SiC [18] and GaN in both structures [19] and for WZ AlN [20]. There are differences, however, in the magnitudes of the band gaps obtained with the earlier empirical pseudopotential calculations [19, 18] in which the gaps were adjusted to experimental data. As is well known, the gaps are underestimated in the LDA Kohn-Sham eigenvalue spectrum. We have calculated a correction to the LDA gap following the approach of Bechstedt and Del Sole [21]. Their method provides essentially a tight-binding estimate of the correction Δ_{GW} to the quasiparticle energy in Hedin's many-body perturbation theory [22]. We see that typically their procedure slightly overestimates the correction. We note that our bandgaps were calculated at the theoretical equilibrium lattice

PRECEDING PAGE BLANK NOT FILMED

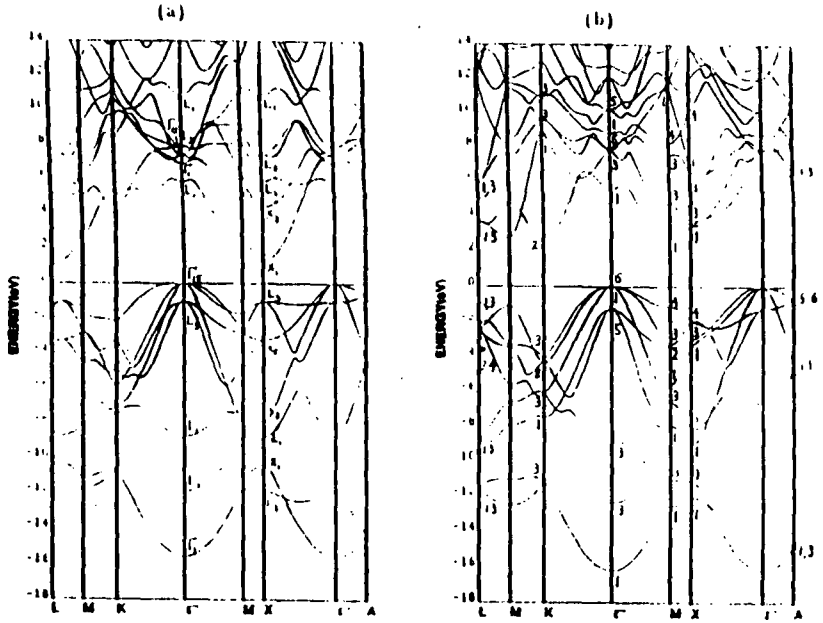

Figure 1: Band structure of SiC in (a) zincblende and (b) wurtzite structure

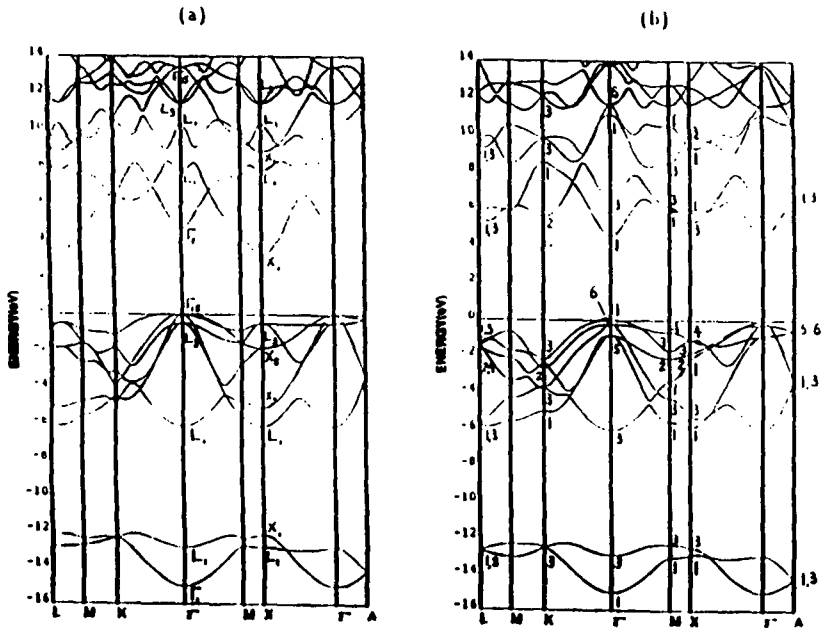

Figure 2: Band structure of AlN in (a) zincblende and (b) wurtzite structure

ORIGINAL PAGE IS
OF POOR QUALITY

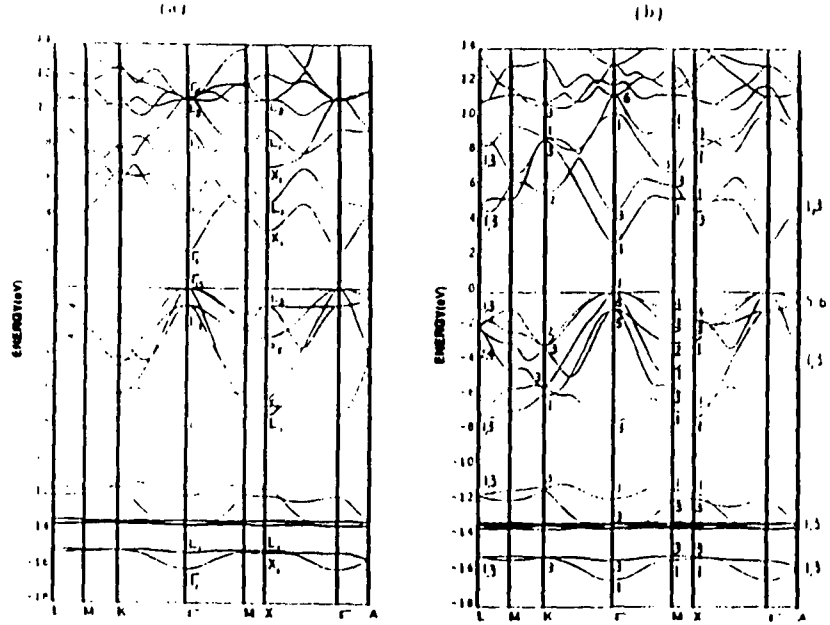

Figure 3: Band structure of GaN in (a) zincblende and (b) wurtzite structure

Table II: Minimum band gaps of SiC, AlN and GaN in zincblende and wurtzite structures (in eV)

	ZB	WZ
SiC	$\Gamma - X$	$\Gamma - K$
LDA	1.47	2.67
LDA+Δ_{GW}	2.7	3.9
Expt.	2.416[a]	3.330[a]
AlN	$\Gamma - X$	$\Gamma - \Gamma$
LDA	3.32	4.94
LDA+Δ_{GW}	5.1	6.7
Expt.		6.28[a]
GaN	$\Gamma - \Gamma$	$\Gamma - \Gamma$
LDA	2.09	2.75
LDA+Δ_{GW}	3.6	4.2
Expt.		3.6[b]

a. Landolt and Börnstein Tables, [17]
b. Bloom et al. [19]

ORIGINAL PAGE IS OF POOR QUALITY

constant using the experimental c/a ratio and the ideal value of u, namely 0.375. This partially explains the discrepancy from Ching and Harmon's value (4.4 eV) for the LDA gap of AlN which was calculated at the slightly larger experimental lattice constant. At the experimental lattice constant and the non-ideal experimental value $u = 0.385$, we obtain 4.6 eV. For GaN, the calculations of Bloom et al. [19] obtained the bandgap for ZB only 0.1 eV lower than that for WZ GaN. They, however, used the same form factors for their pseudopotential calculation, instead of self-consistent quantities for each of the structures.

Next, we consider a number of aspects of the band edges, including the directness or indirectness of the bandgaps. First of all, one may notice that the energy of the X_1^c conduction band minima are lower in ZB than the corresponding states in WZ in all three compounds. This is in part a result of the fact that in ZB the only state of the same X_1 symmetry, with which it can interact, lies quite deep. In a tight-binding picture, the X_1 valence and conduction band states are bonding and antibonding combinations of the anion s-orbital with a cation p-orbital. In WZ, on the other hand, this point has a lower symmetry and the state can interact with several closer lying states. The interaction with the upper valence band states of the same symmetry tends to push the WZ conduction band state to higher energies. There is no interaction with the nearest conduction band state above the minimum because this state has a different symmetry. In addition, the eigenvalues along the $M - L$ axis must approach each other to become degenerate at L on the face of the Brillouin zone, because the spacegroup (C_{6v}^4) is non-symmorphic. This also tends to push up the conduction band edge at X in WZ.

In AlN, the competing level for the conduction band minimum is the Γ_1 state. Thus, that state becomes the conduction band minimum in WZ, and, although it falls just barely below the lowest conduction band state at the X-point, the gap becomes direct. In the case of SiC, however, the Γ_1^c conduction band state is higher in energy relative to the eigenvalues at the other k-points and thus does not become the minimum in WZ. Rather, it is the K-point where the minimum occurs, followed closely (at 0.12 eV higher) by the M-point. This leaves the band gap indirect. The energies of the conduction band minimum at the M-point are practically the same in the ZB and WZ structures, but the K-point is lowered by about 1 eV. The fact that the conduction band minimum changes character because of these symmetry effects, explains why there is a significant difference in band gap (by about 1 eV) between the cubic and hexagonal SiC polytypes.

Finally, we may inquire as to why the Γ_1^c state is relatively higher (with respect to conduction band states at other k-points) in SiC and lower in GaN compared to AlN. Those facts prevent SiC from becoming direct even in WZ and makes GaN direct even in ZB. The Γ_1^c state is basically an antibonding combination of cation and anion s-orbitals. As such it is quite sensitive to the depth of the potential well near the nucleus. Obviously, Ga, being the atom with the highest atomic number, has the strongest potential at the nucleus. The key factor in the comparison between SiC and AlN is the stronger ionicity of the latter. This is confirmed by a partial wave analysis of the Γ_1^c state which shows a smaller admixture of N 2s in AlN than of C 2s in SiC. Since the cation of these compounds have a larger Z than the anions, the higher cation content in AlN more than compensates for the slightly stronger Si potential at the nucleus.

We note that for GaN, it is important to treat the Ga 3d semicore state as a band state. It overlaps in energy with the N 2s band and hybridizes significantly with it at most k-points except Γ. We found that omission of this state leads to a larger equilibrium lattice constant, and, as a result to a lower bandgap (1.8 eV in the LDA).

Finally, we find that the densities of states (DOS) in the WZ and the ZB structures show systematic differences which are very similar in SiC, AlN and GaN. The valence band DOS is more peaked near the top of the band in WZ. These differences should be observable in XPS or UPS photoemission or in soft X-ray emission spectra of the valence band and may also be identifiable in the CVV (core-valence-valence) Auger electron spectra of these materials. The latter essentially corresponds to an auto-convolution of the valence band density of states. This may be useful for the experimental characterization of the cubic versus the hexagonal structure.

CONCLUSIONS

Using the LMTO-ASA method we have calculated the band structures and equilibrium properties of SiC, AlN and GaN in the zincblende and wurtzite structures. We have discussed the origin of the directness and indirectnes of their bandgaps.

This work was supported by ONR and the N.A.S.A. Lewis Research Center.

REFERENCES

1. W. Seifert and A. Tempel, *Phys. Status Solidi (a)* **23**, K39 (1974).
2. D. Schwabe and W. Mader, in *Proceedings of the European Conference on Advanced Materials and Processes (EUROMAT)*, Aachen, Germany, Nov. 22-24, 1989.
3. P. Hohenberg and W. Kohn, *Phys. Rev.* **136**, B864 (1964); W. Kohn and L. J. Sham, *ibid* **140**, A1133 (1965).
4. U. von Barth and L. Hedin, *J. Phys. C* **5**, 1629 (1972).
5. O. K. Andersen, *Phys. Rev. B* **12**, 3060 (1975); O. K. Andersen, O. Jepsen, and M. Sob in *Electronic Band Structure and its Applications*, edited by M. Yussouff, (Springer, Heidelberg, 1987).
6. J. H. Rose, J. Smith and J. Ferrante, *Phys. Rev. B* **28**, 1835 (1983).
7. R. W. G. Wyckoff, *Crystal Structures*, Second Edition, (Interscience Publishers, New York 1964), Vol. 1.
8. CRC Handbook of Chemistry and Physics, edited by R. C. Weast, (CRC Press, Inc., Boca Raton, FL 1988), 68th Edition.
9. R. D. Carnahan, *J. Am. Ceram. Soc.* **42**, 254 (1959).
10. W. Wettling and J. Windscheif, *Solid. State Commun.* **50**, 33 (1984).
11. D. Gerlich, S. L. Dole and G. A. Slack, *J. Phys. Chem. Solids* **47**, 437 (1986).
12. M. Methfessel, *Phys. Rev. B* **38**, 1537 (1988); M. Methfessel, C. O. Rodriguez, and O. K. Andersen, *Phys. Rev. B* **40**, 2009 (1989).
13. W. R. L. Lambrecht, B. Segall, M. Methfessel, and M. van Schilfgaarde, *Phys. Rev. B* **44**, 3685 (1991).
14. C. Cheng, R. J. Needs, and V. Heine, *J. Phys. C* **21**, 1049 (1988).
15. A. Muñoz and K. Kunc, *Phys. Rev. B* **44**, 10372 (1991).
16. M. R. Salehpour and S. Satpathy, *Phys. Rev. B* **41**, 3048 (1990).
17. *Numerical Data and Functional Relationships in Science and Technology*, edited by O. Madelung, Landolt-Börnstein, New Series, Group III, Vol. 17a (Springer, Berlin, 1982).
18. L. A. Hemstreet and C.Y. Fong, in *Silicon Carbide – 1973*, edited by R. C. Marshall, J. W. Faust, C. Y. Ryan, (University of South Carolina Press, Columbia, SC 1974), p. 284.
19. S. Bloom, G. Harbeke, E. Meier, and I. B. Ortenburger, *Phys. Status Solidi (a)* **66**, 161 (1974).
20. W. Y. Ching and B. N. Harmon, *Phys. Rev. B* **34**, 5305 (1986).
21. F. Bechstedt and R. del Sole, *Phys. Rev. B* **38**, 7710 (1988).
22. L. Hedin, *Phys. Rev.* **139**, A796, (1965).

Ref. 5

ELECTRONIC STRUCTURE AND RELATED PROPERTIES OF TETRAHEDRALLY BONDED WIDE-BAND-GAP MATERIALS CONTAINING EARLY ELEMENTS OF THE PERIODIC TABLE

W. R. L. LAMBRECHT, C. H. LEE, K. KIM, A. G. PETUKHOV, E. A. ALBANESI AND B. SEGALL
Department of Physics
Case Western Reserve University
Cleveland, OH-44106-7079

1. Introduction

The tetrahedrally bonded materials involving early elements of the periodic table, such as Be, B, C, and N have rather extreme properties compared to the conventional tetrahedrally bonded semiconductors. These unique properties make them interesting for a variety of applications, including their use as hard coatings for mechanical tools, metal/ceramic composites, heat-sinks, and electronics. The latter are the most demanding type of applications because they require semiconductor grade purity single crystalline material in order to realize the superior performance these materials promise to have. But their extreme properties also makes them difficult materials to grow in the form of pure single crystals. Their properties are thus not yet very well known. In order to make a rational choice of material for specific applications, it is necessary to understand the interrelationships between the intrinsic materials properties and the trends in these properties with atomic number, crystal structure, and so on. Virtually all materials properties can in ultimate instance be related to the underlying electronic structure. The purpose of this paper is to describe the basic trends in electronic structure of these materials and some of their related properties. The results presented here are based on a systematic study of the electronic structure of these materials carried out over a number of years in our research group. Although many of the results discussed here were pre-

sented elsewhere they were not included in an overall description of the trends as presented here. Some new results are included as well. Extensive references are provided as a guide to our previous work not covered here in detail.

We first describe some of the relationships between intrinsic properties and their importance for various types of applications. Next, we briefly describe our computational approach. Then, we present calculated results for the groundstate properties such as the equilibrium lattice constants, bond strength, elastic constants, as well as the underlying electronic structure — in particular the band gaps — for a number of materials systems.

We classify the materials as follows:

- materials containing only elements from the second row of the periodic table: diamond, BN, BeO
- related Be compounds: $BeCN_2$ and Be_2C
- polytypes of SiC;
- B-compounds: BN, BP, BAs
- the group III-Nitrides: BN, AlN, GaN, InN;
- related II-IV-N_2 materials;
- alloys among III-N's and heterovalent alloys.

2. Relations among intrinsic properties

Wide-band-gap semiconductors have a number of advantages for electronic applications over conventional semiconductors. Among these are larger breakdown fields, resistance to harsh environments, ability to operate at high-temperatures, and high-thermal conductivity. These various properties are important for a variety of applications where conventional semiconductors fail. For example, in conventional semiconductors, intrinsic carrier concentration at a few 100°C wipe out the effects of doping and make semiconductor devices inoperable. Obviously, since intrinsic carrier generation varies exponentially with the gap, wide band-gap materials have an important advantage in this respect. Intrinsic carrier generation also plays an important role in the time-decay of space charges induced by optical excitation of e.g. an MIS or Schottky diode. This may enable new kinds of semipermanent memory and UV detetectors.

At high temperatures, the formation of various types of defects also start to degrade the material. For example, dislocation movement proceeds by kink formation and migration. Vacancy and interstitial production also have a thermal activation energy. All these processes require bond breaking and thus the stronger the covalent bond the more resistant the materials are to high-temperature degradation of the crystalline quality. The wide-band-gap materials we will consider here derive their wide gaps from strong

ORIGINAL PAGE IS
OF POOR QUALITY

covalent bonding and not exclusively from high ionicity. They are thus also strongly bonded. This is also what gives these materials resistance to radiation damage.

The above effects are not only important for high-temperature operation but also for high-power and high-frequency applications. In fact, both of these lead to generation of heat. The thermal conductivity is thus another important performance parameter for a semiconductor. The wide-band-gap tetrahedrally bonded materials have a high phonon-mediated thermal conductivity because of their high sound velocities, which in turn are closely related to the stiffness of the bonds. The latter can best be described in terms of bond strengths, elastic constants and the force constants involved in certain phonon modes.

Another important parameter for high-speed electronics is the static dielectric constant. This is because in a very general sense, electronic devices are based on the transfer of charges from one spatial area to another and thus involve capacitance. One clearly wants as low a dielectric constant as possible. Also good insulators with low dielectric constant are required for isolating various active parts of a device from each other. Thus, as one starts to use wider gap semiconductors, one also needs even wider gap insulators for packaging applications. The electronic dielectric constant at frequencies above vibrational frequencies ϵ_∞ is roughly inversally proportional to the band gap. In partially ionic materials, the static dielectric constant involves also a contribution from the ionic motions. Thus ionicity is an important parameter. Ionicity can be defined in terms of the ratio of the atomic energy level difference to the effective gap between bonding and antibonding states. Phillips' ionicity f_i [1] is related to Harrison's [2] polarity α_P by $f_i = \alpha_P^2$ with

$$\alpha_P = |E_c - E_a|/\sqrt{|E_c - E_a|^2 + 4\beta^2}. \quad (1)$$

Here E_c and E_a are cation and anion atomic energy levels and β is the covalent interaction between sp^3 orbitals pointing towards each other. The quantity $E_G = \sqrt{|E_c - E_a|^2 + 4\beta^2}$ can be interpreted as an average effective gap between cation and anion levels. Effective values for these levels can be extracted from our first-principles calculations [3] and define an ionicity scale. The ionicities of some of the materials discussed here are given in Table 1.

The underlying reason for the unique properties of the materials involving early elements of the periodic table can be understood on the basis of the simple molecular bond picture embodied in Eq.(1). Because of the absence of lower energy p-like orbitals in the core, the 2p levels are anomalously deep compared to 3p levels. Also, 2s levels feel the nucleus more strongly than 3s electrons because the nucleus is less effectively screened by the small core consisting only of 1s electrons. This relatively compact

TABLE 1. Polarities calculated from LMTO-ASA calculations for equal cation and anion sphere sizes

SiC	0.473				
		BN	0.475	AlN	0.807
		BP	0.018	GaN	0.771
		BAs	0.019	InN	0.792
BeO	0.818	BeC*	0.588	BeN*	0.701

* Individual bond polarities in $BeCN_2$.

nature of the 2s and 2p orbitals is responsible for the small lattice constant and strong covalent bonding. The strong covalent interaction β leads to a large effective gap E_G.

When atoms of the second row are combined with atoms of the third row, there is also an anomalous difference in atomic energy levels. This leads to a strong ionic component to the bonding for SiC (even though the latter is a IV-IV compound) and AlN and a surprisingly low ionicity for BP. The latter occurs because the 2p level of B is sufficiently deep that its position approaches that of the P 3p level. By Eq.(1) that implies low ionicity. In fact, taking into account that the effective charge on the V-element is given by $q = 1 - 4\alpha_P$, one finds that it actually has positive charge when $\alpha_P < 1/4$. This is the case for BP and BAs which as a result have inverted ion character: P or As behave as cation while B behaves as anion despite the fact that normally the group-III element behaves as cation and the group-V element as anion. On the other hand, the enhancement of ionicity due to the deep 2s and 2p levels for SiC and III-N compounds contributes significantly to their large gaps.

The relative extent of 2p versus 2s orbitals compared to those of 3s and 3p has another important effect. It implies that there is less advantage in promoting a 2s electron to a 2p orbital to form directed bonds. In fact, strong bonds can also be realized by means of π bonding between 2p-orbitals directly. This means that for elements from the second row of the periodic table there tends to be a competition between tetrahedral bonding and planar sp^2 plus π bonding. Thus, C and BN have competing layered structures: graphite and h-BN. BeO does not exhibit such structures [4] which is related to the higher ionicity of this II-VI compound. Indeed ionicity tends to favor higher coordination.

Ionicity also plays a role in the relative stability of cubic versus hexagonal stacking of tetrahedrally bonded layers [5]. Thus, the relatively low ionicity compounds BP, BAs and BN and (zero ionicity) elemental C fa-

for the cubic structure while the III-nitrides have wurtzitic structures and SiC exhibits polytypism. Ionicity plays also an important role in electronic transport. The polar mode scattering increases with increasing effective charges.

Wide band gaps have another important application in optoelectronics where they extend the range of light emission frequencies into the blue and UV. In this context, it is important whether the gap is direct or indirect. Other important parameters for electronic applications are effective masses, deformation potentials, and other band structure details. Some examples will be discussed below.

Finally, an important aspect of potential semiconductor materials is the possibility of doping the material n and p-type. Diamond has proved to be quite difficult to dope n-type. GaN was difficult to dope p-type although effective p-type doping with Mg was recently achieved using post-doping annealing and Low energy electron beam irradiation (LEEBI) treatments [6]. AlN has sofar resisted effective doping of either type. BN has been reported to be both n and p-type dopable [7]. Although this is an important issue, we will not discuss it further because we have not done studies of this aspect in our group.

In summary, we have here given some examples of how the electronic, structural and bonding properties are interrelated and how they impact device applications. In the remainder of the paper we focus on the electronic structure.

3. Computational Method

The theoretical framework of our first-principles calculations is density functional theory [8]. This approach basically reduces the many-body problem of interacting electrons to that of independent electrons in an effective potential with the same ground state electron density as the real system. The total energy of the system is expressed in terms of the Coulombic energy of the electron charge density and the positively charged nuclei, the kinetic energy of the independent model electron system and a remainder which is called the exhange-correlation energy. The method is in principle restricted to the study of groundstate properties. The local density approximation (LDA) allows one to incorporate effects of exchange and correlation in a mean-field approximation. It assumes the same functional form for the exchange-correlation energy as in the homogeneous electron gas but applies it locally to each volume element of the real inhomogeneous system: $E_{xc} = \int e_{xc}[n(\mathbf{r})]n(\mathbf{r})d^3r$. We use the parameterization of the exchange and correlation functionals by Hedin and Lundqvuist [9].

An important point to realize about this theory is that the eigenvalues

ϵ_{nk} of the effective one-electron Schrödinger equation

$$[-\frac{\hbar^2}{2m}\Delta + v_H(\mathbf{r}) + v_{xc}(\mathbf{r})]\psi_{nk}(\mathbf{r}) = \epsilon_{nk}\psi_{nk}(\mathbf{r}). \quad (2)$$

where v_H is the Hartree potential combining the electron and nuclear electrostatic potential, and v_{xc} is the exchange-correlation potential. do not have the meaning of single particle excitations. For a periodic solid the ϵ_{nk} constitute the band structure. In other words the band structures we calculate in this theory form a useful construct to understand total energy properties and bonding but do not represent the energies required to extract electrons from the system as measured for example by photoemission or as involved in optical excitations (excluding excitonic effects). The true quasiparticle excitations are given be the related equation:

$$[-\frac{\hbar^2}{2m}\Delta + v_H(\mathbf{r})]\Psi_{nk}(\mathbf{r}) + \int \Sigma_{xc}(\mathbf{r}, \mathbf{r}', E_{nk})\Psi_{nk}(\mathbf{r}')d^3r' = E_{nk}\Psi_{nk}(\mathbf{r}). \quad (3)$$

with $\Sigma_{xc}(\mathbf{r}, \mathbf{r}', E_{nk})$ the non-local and energy dependent exchange-correlation self-energy operator. In practice, however, the wavefunctions of the two equations are quite close to each other and the effects of replacing the v_{xc} by Σ_{xc} can be treated by perturbation theory. The self-energy operator can be approximated by Hedin's GW approximation [10]. Carrying out this calculation in practice is rather cumbersome and has been done for only a few systems [11, 12, 13, 14]. The main finding, however, is that the spectrum of E_{nk} and ϵ_{nk} mainly differ by a gap correction which is roughly k-independent and energy independent. The latter can actually be estimated easily by means of an approximate treatment of the above theory proposed by Bechstedt and Del Sole [15].

The fact that LDA band structures underestimate the gap is well known as the "gap problem". It is actually not a failure of LDA but a question of appropriately interpreting the theory. The GW approximation predicts the correction to be only weakly dependent on crystal structure. Thus LDA band structures ϵ_{nk} can be used to investigate changes in band structure with crystal structure. The GW calculations actually also predict a small rigid shift of the bands with respect to the average electrostatic potential. This is irrelevant for most purposes, because one is usually interested only in interband differences, but it does have an effect on the band-alignment at a heterojunction. The magnitude of this shift appears to depend somewhat on the actual choice of parametrization of the LDA exchange correlation potential and to that extent is not yet well established theoretically [12]. While for wide bands the only important correction appears to be the above described gap correction, narrow bands such as core and semi-core levels

are subject to additional self-energy corrections. This is e.g. important for Ga 3d states in GaN [16].

The method we use to calculate the energy bands, i.e. to solve Eq.(2) and obtain the self-consistent potential, is the linear muffin-tin orbital method [17]. Most of the results reported here were obtained in the so-called atomic sphere approximation (ASA) in which Wigner-Seitz spheres replace the actual Wigner Seitz cells and a spherical approximation is made to the charge density and potential inside each sphere. This method is in very good agreement with the so-called full-potential calculations which do not make this approximation except for quantities which involve small energy differences or in cases where significant distortions of the local spherical symmetry occur. For example, cohesive energies, lattice constants, bulk moduli and band structures are usually given quite accurately by the ASA. Surface energies and workfunctions, however, are not because of the strong non-spherical dipole potential near a surface. In fact, the main problem with the ASA is in the spherical approximation to the charge density rather than to the potential. The errors induced by using slightly overlapping spherical charge densities can to a good extent be corrected by means of the so-called Ewald correction [17] in which one corrects for the overlap by redistributing the overlap charge into a homogeneous background charge. We have used this approach successfully in our structural energy minimizations for the chalcopyrite II-IV-N_2 compounds [18]. For the calculation of optical phonon frequencies and elastic constants, which require the calculation of very small energy differences in order to stay within the linear response regime with respect to the strain or phonon distortion perturbation, we need full-potential calculations. The latter were done using the approach of Methfessel [19].

Our approach for dealing with disorder in alloys and other specifics will be described along with the results in the appropriate sections.

4. Results

4.1. DIAMOND, BN, AND BEO.

In Table 2, we present calculated lattice constants, bulk moduli, bond strengths (defined as 1/4 of the cohesive energy per zincblende unit cell with respect to free (spin-polarized) atoms), and band gaps for diamond, BN, and BeO. We include calculations both for the cubic and hexagonal crystal structures: i.e. cubic diamond and lonsdaleite diamond and zincblende and wurtzite for the other binary compounds. Our results for hexagonal diamond and BN are are in good agreement with those of Salehpour and Satapathy [21] and Gorczyca and Christensen [22] respectively, but are more complete. (Not all quantities given here are provided in the above ref-

erences.) We note that the groundstate equilibrium properties are similar in the hexagonal and cubic forms. The present ASA calculations, however, are not sufficiently accurate to determine the relative stability of the wurtzite and zincblende structures. In addition, special care has to be taken in using equivalent k-point sets and in relaxing the internal degree of freedom to establish this small energy difference. That would require full-potential calculations. The structure determination was not the primary purpose of the present study. We also note that typical errors for bulk moduli are 10 %. The ~10 % difference in bulk modulus between cubic and hexagonal diamond and c-BN is probably overestimated in part because we did not relax the structural degrees of freedom, i.e. the relative position of the two sublattices and the c/a ratio in hexagonal structure, which are not determined by symmetry. The overestimate of the bulk modulus is consistent with the underestimate of the lattice constant and overestimate of the bond energy. The band gaps of the hexagonal crystals, however are expected to be quite accurate.

TABLE 2. Properties of diamond, BN, BeO and $BeCN_2$: lattice constants (a_c for cubic, a_h and c/a for hexagonal) (Å), bulk modulus B (GPa), bond energy E_b (eV), and minimum band gap E_g (eV).

		cubic			hexagonal			
		theory	expt.		theory	expt		
Diamond	a_c (Å)	3.58	3.567		a_h (Å)	2.46	2.522[a]	
					c/a	1.633[a]		
	B (GPa)	434	442		B (GPa)	506		
	E_b (eV)	4.2	3.7		E_b (eV)	4.7		
	E_g (eV)	4.4	5.5	$\Gamma - \Delta$	E_g	3.6	(4.7)[b]	$\Gamma - K$
BN	a_c (Å)	3.62	3.616		a_h (Å)	2.51	2.56	
					c/a		1.633[a]	
	B (GPa)	381	290-465		B (GPa)	425		
	E_b (eV)	3.8	3.3		E_b (eV)	4.2		
	E_g (eV)	4.5	6.4	$\Gamma - X$	E_g (eV)	5.7	(7.6)[b]	$\Gamma - K$
BeO	a_c (Å)	3.80	3.79		a_h (Å)	2.64	2.664	
					c/a	1.633[a]	1.623	
	B (GPa)	224			B (GPa)	248	224-249	
	E_b (eV)	3.4	3.0		E_b (eV)	3.7	3.0	
	E_g (eV)	6.9	(9.3)[b]	$\Gamma - X$	E_g (eV)	8.3	10.7	$\Gamma - \Gamma$

[a] assuming ideal $c/a = \sqrt{8/3}$

[b] estimate assuming gap correction to be independent of structure

The band gaps depend significantly on the structure. Even the k-point location of the conduction band minimum changes. In Fig. 1 we show how some of the conduction-band eigenvalues relative to the valence band maximum change across the series. One may note that the s-like Γ_1 states in both cubic and hexagonal structures come down in the series while the Γ_6 state of hexagonal and Γ_{15} state of cubic move up. M_h and K_h states of the hexagonal structure also move up toward BeO. One can relate the k-points of the cubic fcc and hexagonal hcp Brillouin zones by assuming the $[111]_c$ direction to be equivalent to the $[0001]_h$ direction and the $[110]_c$ direction to be equivalent to the $[11\bar{2}0]_h$ direction [23, 24]. The cubic X point corresponds to the point 2/3 along M-L_h and is different from K_h. We note that in all cases going from cubic to hexagonal the X conduction band minimum moves up in energy and the K minimum comes down. This is thus a structure related effect. In the case of BeO, however, the Γ minimum is lower in energy than K_h and thus leads to a direct gap material. We also note that the gap in hexagonal diamond is lower than in cubic while the inverse is true for BN and BeO. The bond energy and bulk moduli decrease across the series diamond-BN-BeO while the lattice constant increases. Both hexagonal diamond and wurtzitic BN appear to be metastable phases. It is not clear whether there is a stability region in the phase diagram or whether their occurence is due only to kinetics. The latter appears to be the case since hexagonal diamond has sofar only been formed under shock compression conditions. BeO is only known in the wurtzitic phase. This is consistent with its high ionicity. The cubic phase is significantly higher in energy (0.14 eV/atom according to Chang et al. [25]) and is unlikely to be formed.

Relation to graphitic structures We note that diamond and c-BN have competing layered structures graphite and h-BN, which are actually the equilibrium phases at ambient pressures. As shown by Fahy et al. [28, 29] the energy differences between the layered forms and the tetrahedrally bonded forms are small but there is a large energy barrier which impedes the transition from one phase to the other. In their models, the transition path from rhombohedral graphite to diamond, or h-BN to wurtzite BN corresponds to a gradual decrease of the distance between the layers which then start to buckle. Layered phases of BeO have been shown to be unstable by Wentzcovitch et al. [4].

Diamond tetrahedral bonding, however, can also be stabilized by surface hydrogen. Hydrogenation of aromatic molecules yields buckled tetrahedrally bonded rings. Similarly, graphite sheets start to form buckled rings when hydrogenated from the edges inwards. This leads to a curling or bending of the planes [30] and to the formation of a diamond-like structure on

ORIGINAL PAGE IS
OF POOR QUALITY

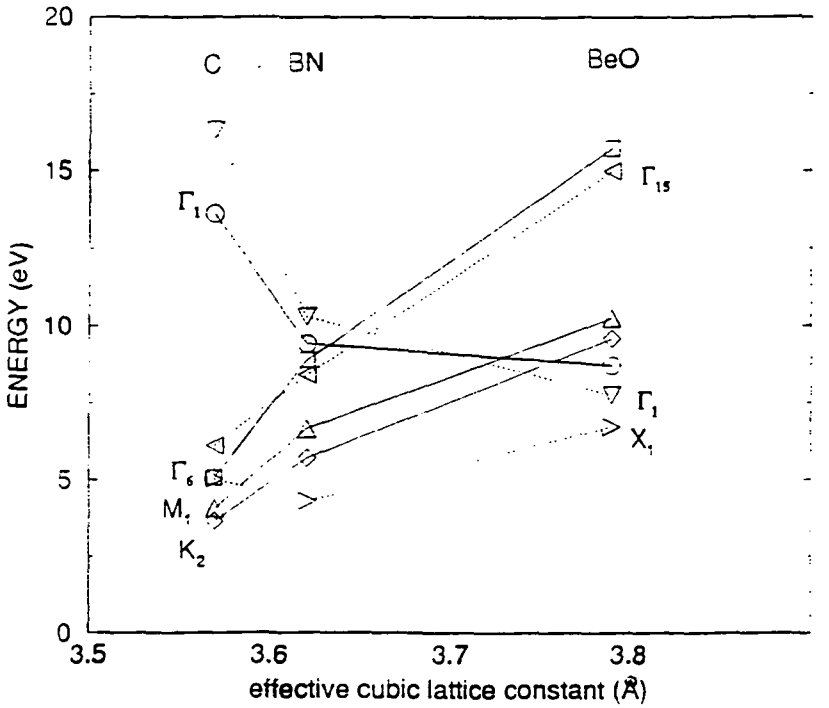

Figure 1. Conduction band eigenvalues of diamond, BN and BeO versus effective cubic lattice constant. Full lines and symmetry notation on the left refer to the hexagonal structure, dotted lines and symmetry notation on the right refer to the cubic structure.

the prism planes of graphite. This is suggested by the open circles in Fig. 2 which shows the calculated structure at the prism plane interface between graphite and diamond. That relaxed structure was calculated [31] using the semi-empirical Tersoff potential [32]. It was conjectured by Lambrecht *et al.* [31] to form a critical step in the nucleation of diamond.

Interfaces We have also studied interfaces between some of these materials: diamond/c-BN [20], diamond/BeO [33] and diamond/Cu [34]. We found that the diamond/c-BN offset is of type II, i.e. the valence and conduction band of diamond are both above those of c-BN. This also has importance for alloys, as will be discussed below. The bonding at these interfaces is quite strong because there are no dangling bonds and the valence bands of the materials overlap each other in a wide energy range. In contrast, the bonding at Cu/diamond interfaces is much weaker because the Cu3d-band is narrow and essentially only the Cu4s bands form bonds with the diamond dangling bonds. An important quantity is the adhesion energy W_a, which

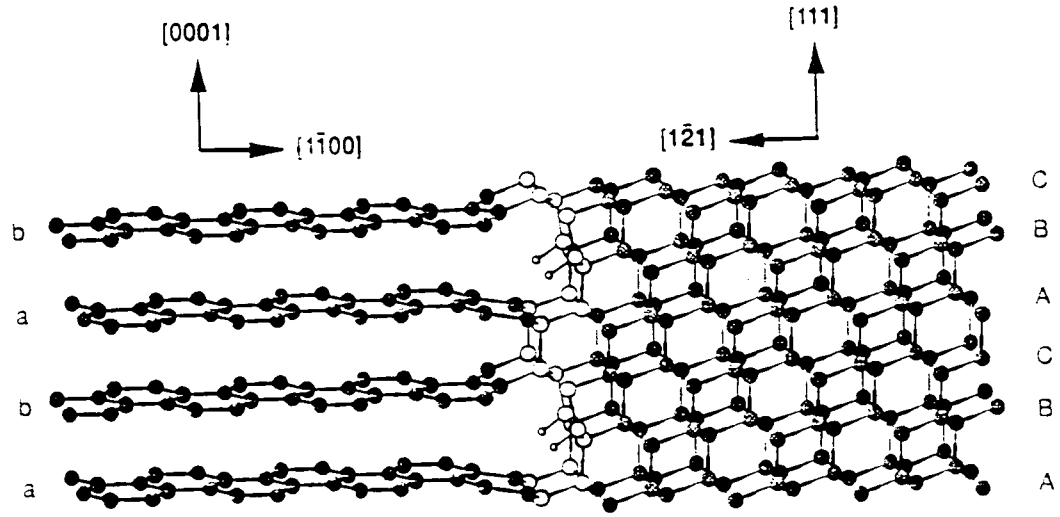

Figure 2. Structure of the prism plane interface between graphite and diamond. Three layers of diamond almost perfectly match two layers of graphite. Hydrogen atoms (small circles) satisfy the dangling bonds of the "non-bonded" diamond layers. The structure at the interface (open circles) indicates that the curling of buckled rings forms an initial diamond nucleus.

is given by

$$2W_a = \gamma_A + \gamma_B - \gamma_i, \tag{4}$$

where γ_A, γ_B are the surface energies of the materials brought together at the interface and γ_i is the interface energy. For diamond/Cu, the adhesion is much weaker than for the interfaces of diamond with c-BN and BeO, mainly because the Cu surface energy is so much smaller than that of these tetrahedrally bonded materials. Surface energies basically scale with cohesive energies because they involve bond breaking. Table 3 gives the calculated surface energies and adhesion energies. Details can be found in [20, 33, 34].

The suitability of c-BN and BeO as substrates for heteroepitaxial diamond growth was confirmed by several experimental studies [35, 36, 37]. While fully developed epitaxial films could be grown on c-BN [36], only oriented growth of particles of size up to about 10 μm in diameter and with slight misorientations of a few degrees has been realized sofar on BeO. This is consistent with the better lattice match and adhesion energy to c-BN.

TABLE 3. Surface and adhesion energies (in J/m^2).

diamond ideal (110) surface energy	6.5
c-BN ideal (110) surface energy	5.2
zincblende BeO ideal (110) surface energy	4.8
diamond/c-BN adhesion energy	5.4
diamond/BeO adhesion energy	4.6
diamond 2×1 (111) surface energy	5.5
Cu (111) surface energy	2.0
diamond/Cu adhesion energy	2.3

4.2. RELATED BE COMPOUNDS: BE_2C, BE_3N_2 AND $BECN_2$

Besides the elemental IV, III-V and II-VI materials of the second row of the periodic table, three other compounds with tetrahedral or closely related bonding are of interest: $BeCN_2$, Be_2C, and Be_3N_2. The main properties obtained in our calculations for the first two of these are given in Table 4.

TABLE 4. Properties of $BeCN_2$ and Be_2C.

	$BeCN_2$	Be_2C
Structure	chalcopyrite	antifluorite
Lattice constant a (Å)	3.71	4.29 (4.342)[a]
c/a	1.96	
u[b]	0.30	
Bulk modulus B (GPa)	333	213
Cohesive energy (eV/atom)	7.7	6.0
Band gap (eV)	4.2 (6.3)[c]	1.15 (2.15)[c]
	direct $\Gamma - \Gamma$	indirect $\Gamma - X$

[a] expt. value in parentheses
[b] u is the internal displacement parameter of the chalcopyrite structure [18]
[c] With estimated gap correction based on interpolation for related materials.

Beryllium carbonitride $BeCN_2$ is todate a hypothetical material [26, 18], which is here assumed to have the chalcopyrite structure in analogy with other II-IV-V_2 compounds such as $ZnGeP_2$. One may think of it as being derived from BN by replacing every other B (group-III) by a Be (group-II) or a C (group-IV) atom. This substitution maintains the local stoichiometry because each N atom is surrounded by two Be and two C atoms. The

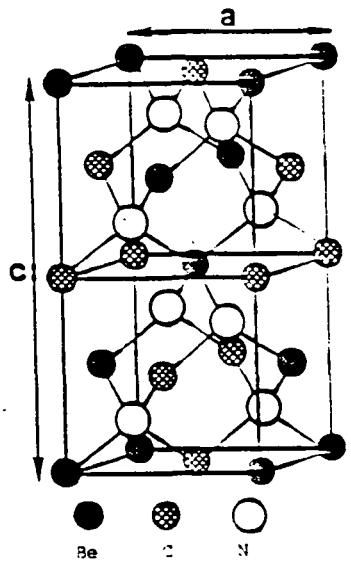

Figure 3. Chalcopyrite structure assumed for the hypothetical material $BeCN_2$. The structure represented here is idealized. Bond lengths relax by a relative motion of the N sublattice towards C and away from Be. If Be and C atoms are both replaced by B we obtain the zincblende stucture of c-BN.

structure is shown in Fig. 3. The bonding in this material is tetrahedral. There are several interesting things about this material.

- It has a lattice constant intermediate between those of c-BN and BeO and may thus form a good bufferlayer for diamond or c-BN growth. We note that it is more ionic than c-BN and may thus, as BeO, be more likely to avoid layered sp^2 bonded structures.
- It has a pseudodirect band gap in the sense that the "directness" results from the fact that the zincblende X point is folded onto Γ in the chalcopyrite structure. A strong mixing of Γ and X states, however, is expected to occur due to the significant difference between Be and C potentials and, in addition, due to the lattice distortions. This should lead to a significant dipole matrix element and thus strong light-emission.
- Related materials such as $ZnGeP_2$ are promising for non-linear optics applications [27] due to the occurence of IV-V bonds. If, as is expected, similar non-linear optical advantages of the C-N bonds occur here, they would be of particular interest because the band gap is already in the UV.

Be_2C A material with bonding closely related to tetrahedral bonding is Be_2C. It has the cubic antifluorite structure. The latter consists of a fcc sublattice of carbon atoms with Be atoms occupying all tetrahedral interstitices. In the zincblende structure by contrast, only half of the tetrahedral interstices of the fcc lattice are filled with a counter ion. We have calculated the ground state properties and band structure of this material [38]. The main results are given in Table 4. The material is an indirect semiconductor with band gap and lattice constant close to those of 3C-SiC.

Formation energies Under atmospheric conditions Be_2C is unstable towards formation of $Be(OH)_2$ by reaction with water vapor, or BeO with O_2. This indicates that Be_2C is less stable than $Be(OH)_2$ or BeO. Nevertheless, a small amount of Be_2C formation was detected in growth expriments of diamond on BeO [37]. This indicates that in spite of the much smaller formation energy of Be_2C than that of BeO, Be_2C can form under the very reducing conditions of diamond growth. This is significant for the prospects of synthesising $BeCN_2$. Our calculations predict a much higher energy of formation for this material, close to that of BeO. The energies of formation, defined with respect to the elements in their standard state and being positive in the case of exothermic reactions, i.e. when the compound has lower energy than the sum of the energies of the elements, are given in Table 5. They were calculated by combining our LDA calculated cohesive energies of the respective solids with LDA binding energies of the molecules O_2 and N_2 given by Jones and Gunnarsson [39]. In this way, the systematic LDA overestimate of bonding is cancelled out. The energy of carbon was taken to be that of diamond instead of graphite, the latter being almost equal in energy. Zero point motion corrections were not included in our cohesive energies because for the present purpose, we only need a qualitative estimate. We note that a large part of the stabilization energy of $BeCN_2$ is due to the effective relaxation energy of 1.2 eV/atom. The related material Be_3N_2 is included in this table. Its structure is an ordered vacancy structure of the antifluorite structure. One may see that per equivalent amount of Be atoms, i.e. 1/3 mole of Be_3N_2, its energy of 47 kcal is also much smaller than that of $BeCN_2$. This indicates that under reaction conditions where either Be_2C plus N_2, or Be_3N_2 plus graphite, or $BeCN_2$ could form, the last is most likely in a thermodynamic sense. It indicates that when Be is exposed to C and N simultaneously, $BeCN_2$ may form exothermically. This calculation, being strictly thermodynamic, of course, does not tell us anything about possible reaction barriers.

TABLE 5. Exothermic energies of formation (in kcal/mole) of some Be compounds.

	theory	expt.
BeO	158	145
1/2 Be_2C	14.5	14
1/3 Be_3N_2		47
$BeCN_2$	156	

4.3. SILICON CARBIDE

Silicon carbide is unique among the wide-band-gap semiconductors in the sense that it exhibits polytypism. Over a hundred different crystal structures called polytypes have been discovered [40]. All are tetrahedrally bonded but differ in the stacking of what are the {111} planes in cubic SiC (called 3C-SiC or β-SiC) and the basal planes {0001} in hexagonal or rhombohedral SiC, sometimes collectively denoted α-SiC. The polytypes can most easily be described as a periodic structure of twin boundaries in cubic SiC. When a twin boundary occurs every 3 (2) layers, we obtain ⟨3⟩ (⟨2⟩) which is the Zhdanov notation [41] for 6H-SiC (4H-SiC). When they occur every layer we obtain the wurtzite structure which is purely hexagonal and denoted 2H-SiC or ⟨1⟩. Rhomobohedral polytypes exhibit more complex patterns such as ⟨32⟩ or 15R.

The relative stability of the various polytypes has been studied extensively by Heine et al. [42]. Some of the main conclusions of their work is that polytypes with bands of three and two layers between twin boundaries (e.g. 6H, 4H, 15R) are most stable, followed by 3C SiC, while least stable is 2H-SiC. On the basis of their total energy calculations, they proposed a model in terms of interlayer interactions. The origin of the polytypism in this context is that the first nearest neighbor layer interactions prefer to stack cubically with respect to each other while the second nearest neighbor interaction favors hexagonal stacking and has almost exactly half the magnitude of the first nearest neighbor interaction. The third and higher neighbor layer interactions are found to be negligible. Their model explains the preference for polytypes with bands of two and three successive cubically stacked layers. It also explains why in surface growth, if complete 3D equilibrium is not reached, there is a tendency to form cubic stacking. This occurs because for the surface layer there is only one next neighbor layer interaction to be considered instead of two in the bulk. Finally, small differences in the phonon contribution to the free energy were claimed to be

the origin of different temperature stability regions for 4H and 6H. Experimentally, it is found that polytype selection can be influenced by a number of kinetic factors besides thermodynamic equilibrium. Growth on vicinal surfaces tends to stabilize the same polytype as the substrate on which it is grown through a ledge growth mechanism. Imperfections on large terraces tend to promote independent nucleation and cubic growth. Lower temperatures also tend to lead to cubic growth. All of this is consistent with the notion that there must be sufficient mobility of species on the surface to move to ledges to continue the substrate polytype and that otherwise cubic nuclei tend to form. In case of cubic growth in the [111] orientation one is often faced with the problem of so-called double position boundaries (DPB). The latter correspond to the two equivalent orientations of a cubic nucleus with respect to the substrate. Stress can induce polytpic transformations [43]. Also, ion implantation can influence polytypism after recrystallization of the damaged area [44]. Finally, doping and growth rates may have an influence on which polytypes form during growth [44].

Our own work has focused on the relationship between polytypism and properties. Integrated properties such as elastic constants [45] are only weakly dependent on polytype while band structure depends dramatically on polytype. This is because band structure essentially corresponds to the formation of electronic standing waves and is thus very sensitive to the structure [24]. The changes in band structure also lead to important changes in optical reflectivity [46].

Fig. 4 shows the dependence of the minimum gap and some specific indirect gaps on polytype. The polytypes are here ordered in order of increasing hexagonality, i.e. the proportion of layers that are stacked hexagonally. One may see that changes in the position of the conduction band minimum occur. While the low hexagonality polytypes have their minimum along the hexagonal $M - L$-axis, including the cubic X-minimum, 2H-SiC has its minimum at K similar to hexagonal diamond and BN. One may also notice that the specific gaps do not vary monotonously with hexagonality. Details on how the band structures are related to each other can be found in [24, 23].

Fig. 5 shows the calculated UV-reflectivity spectra of some SiC polytypes compared to experimental data. We note that a single k-independent and polytype independent gap correction of 1 eV as applied. The latter not only provides good agreement for the various peak positions in the reflectivity spectra but also for the minimum gaps given above. This lends support to our statements in the section on computational method that the gap corrections beyond the LDA are relatively structure independent.

The changes in band structure between the polytypes leads to different effective masses, and hence are important for transport [24]. For example,

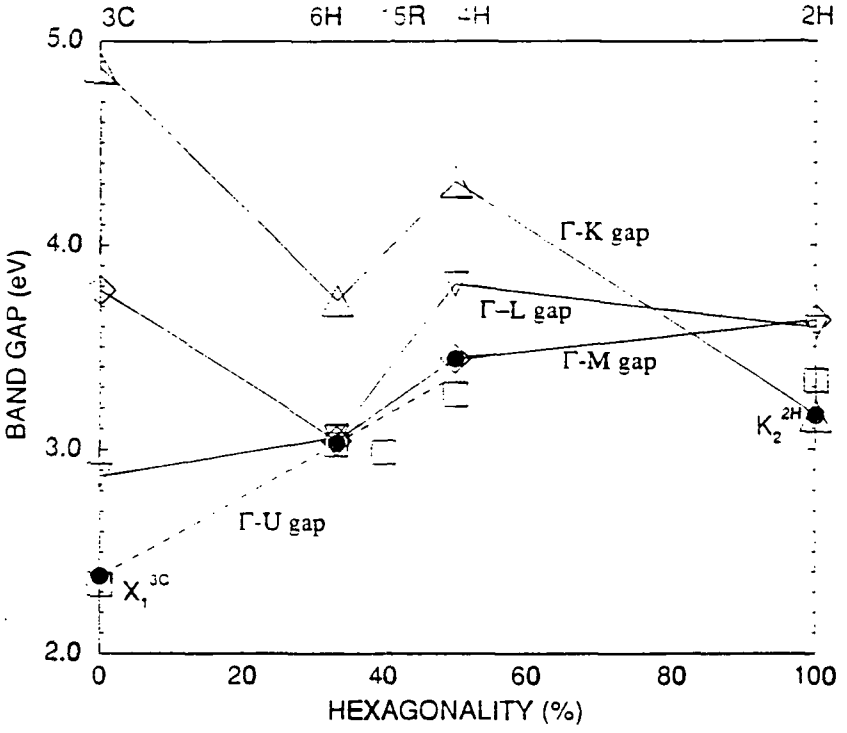

Figure 4. Band gaps of SiC polytypes. Squares: experiment, solid circle: thoeretical minimum gap: diamonds, upward and downward triangles, specific k-point gaps as indicated: dashed line, nearly linear $\Gamma - U$ gap along $U \equiv M - L$ line of hexagonal Brillouin zone.

it is found that 6H SiC has twelve equivalent minima along the $M - L$ axes close to M, which are elongated in the c-direction and with only small barrier between them. This means that at larger temperature the two minima displaced along the c-axis can effectively be thought of as one minimum with a very large mass anisotropy. This is consistent with recent measurements of a large anisotropy in mobilities in 6H-SiC [47].

We have also studied several interfaces involving SiC. SiC/AlN and SiC/BP interfaces [48] will be briefly discussed in the section on alloys because of the close relationship among these topics and the new results we present here on the corresponding alloys. We also studied SiC/TiC interfaces which are of interest for metallization of SiC and in connection with ceramic reinforcement of metals [49]. Finally, we studied so-called inversion domain boundaries in SiC [50]. These are planar defects that occur often during growth on stepped Si {001}.

ORIGINAL PAGE IS
OF POOR QUALITY

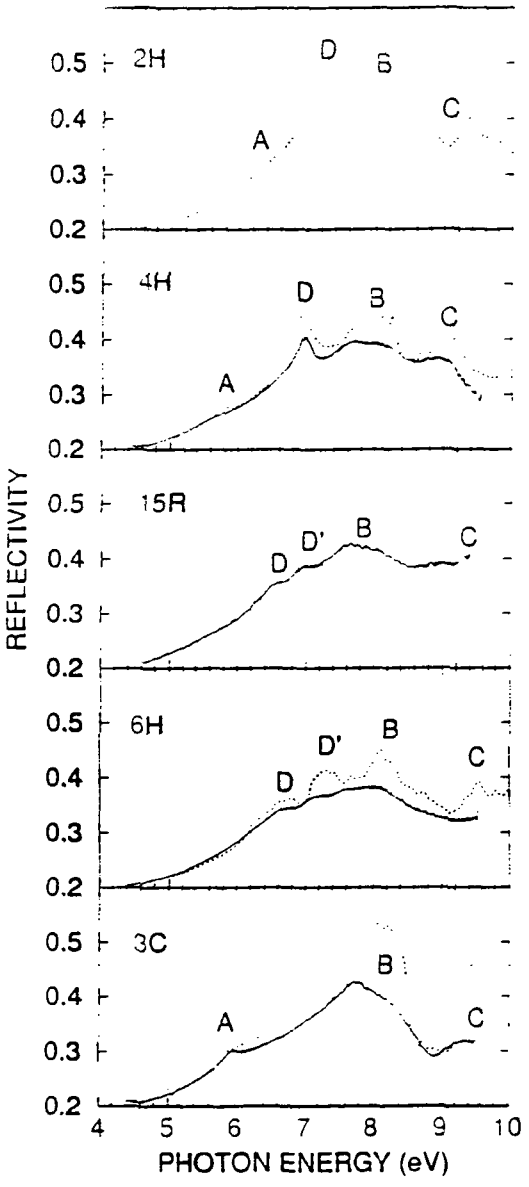

Figure 5. Reflectivity of SiC polytypes. Solid lines experiment, dotted lines theory.

4.4. BORON COMPOUNDS: BN, BP AND BAS

Table 6 presents an overview of boron compounds c-BN, BP and BAs as

TABLE 6. Properties of tetrahedrally bonded boron compounds: a lattice constant. B bulk modulus. E_b bond energy, E_g minimum band gap, and conduction-band minimum location k_{min}.

		a (Å)	B (GPa)	E_b (eV)	E_g (eV)	k_{min}
BN	present	3.62	381	3.8	4.5	X
	PP[b]	3.606	367	3.6	4.2	X
	Expt. [a,b]	3.615	290-465	3.3	6.4	
BP	present	4.51	172	2.8	1.35	Δ
	PP[b]	4.558	165	2.9	1.2	Δ
	Expt.[a,b]	4.538	173-265	2.6	2.4	
BAs	present	4.79	130	2.3	1.06	Δ
	PP[c]	4.777	145	2.6	1.2	Δ
	Expt.[a,c]	4.777	-	-	2.1[d]	

[a] Experimental values from Landolt-Börnstein Tables [53].
[b] Pseudopotential calculation by Wentzcovitch et al. [51]
[c] Pseudopotential calculation by Wentzcovitch et al. [52]
[d] Our estimate assuming correction same as for BP. Expt. values are uncertain.

calculated using the ASA-LMTO method. We have included data on BN, which given above to facilitate the comparison to BP and BAs. The reason why BP in the table below has a slightly underestimated lattice constant while the others have sligthly overestimated values is that the calculation of [48] for BP did not include the so-called combined correction. For the present purposes this is not relevant. Our results are in good agreement with the previous calculations by Wentzcovitch et al. [51, 52], although our values for the gaps differ somewhat. We note the usual "softening" as we go to heavier elements. Due to the very low ionicity mentioned earlier, the BP and BAs compounds have a band structure somewhat similar to Si with the minimum along the Δ axis close to X. Experimental band gaps are not well known. We estimate a gap correction of $\sim$1 eV for both BP and BAs on the basis of their similarity to SiC and Bechstedt and del Sole 's model [15]. We emphasize that the low ionicity is expected to reduce polar scattering which may give these materials an advantage in mobilities.

4.5. GROUP-III NITRIDES

We have performed total energy and band structure calculations for the entire series of Group-III nitrides in both the zincblende and wurtzite structure. The two forms are close in energy and can both be stabilized under suitable epitaxial growth conditions. This has already been realized for GaN and InN but not for AlN. At high pressure the nitrides exhibit a phase tran-

ORIGINAL PAGE IS
OF POOR QUALITY

sition to the rocksalt structure. This is a well known phenomenon due to the increase in ionicity under compression and the tendency towards higher coordination for ionic compounds. It has been studied theoretically by Gorczyca and Christensen [22] and by Muñoz and Kunc [54] and experimentally by Perlin et al. [55], Volstädt et al. [56] and Ueno et al. [57]. Our calculated groundstate properties can be found in [23] while full details on the band structures are given in [58].

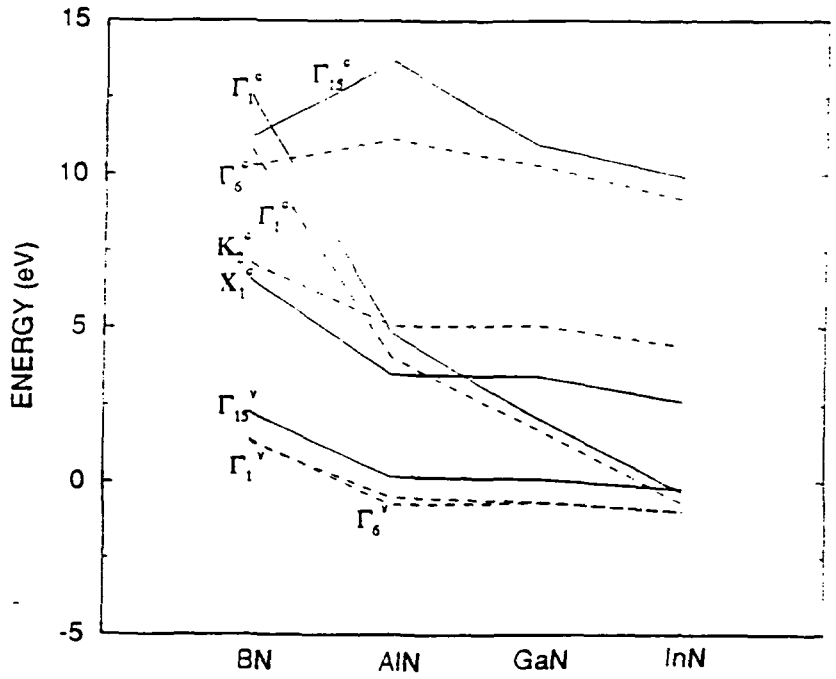

Figure 6. Trends in selected band states of III-nitrides with atomic number in zincblende and wurtzite structure.

Trends in the band structures. The trends of some eigenvalues with cation in the series of nitrides are shown in Fig. 6. It includes the important eigenvalues near the gap, i.e. the valence band maximum Γ_{15}^v for ZB or Γ_1^v and Γ_6^v for wurtzite, the conduction band state Γ_1^c and K_2^c for WZ and X_1^c for ZB which "compete" for the minumum. The conduction band Γ_1^c states in both wurtzite and zincblende are mostly s-like (actually purely s-like in ZB) and, being antibonding states, have important cation-s components. One may see that these states show the largest variation with atomic number, and, in particular, are monotonically decreasing with increasing atomic number.

Of course, the above statement requires that we compare the different band structures with respect to the same reference level. The natural reference level used here is the ASA zero of energy [59] which coresponds to the average of the point charge electrostatic potential and is close to the average potential in the interstitial region. This is not sufficiently accurate to determine band-offsets because that requires consideration of charge transfer. But it is adequate for our present qualitative discussion. The reason for the downward trend with atomic number is well known and also ocurs for example in the series C-Si-Ge-Sn. It is simply due to the fact that s-orbitals have a non-zero value at the nucleus and as such feel the $-Z/r$ potential. Thus, heavier elements have lower s-levels with respect to corresponding p-levels. Since the Γ_1 state is s-like and the X_1^c-level in zincblende (or diamond) is a mixture of s and p-like components and the X_2^c state in wurtzite or lonsdaleite is purely p-like, this explains why diamond, SiC and BN are indirect gap materials in either zincblende or wurtzite structure while GaN and InN are direct in both. AlN turns out to be indirect in the zincblende structure and direct in the wurtzite. Even in WZ, however, the indirect and direct gap in AlN are close to each other in energy. Fig. 6 shows that the variation of Γ_1^c is linear from Al to In but has a different slope between B and Al. This emphasizes again the peculiar role of the second row elements. In addition, the Γ_{15}^c state is lower in c-BN than the Γ_1^c state. This again is a manifestation of the relative energies of p and s-levels and thus a result, once again of the absence of a p-like core for 2p wave functions. We note that the levels shown are LDA levels which are underestimated for the conduction band states as discussed above. Again, however, the LDA is adequate for the study of the structurally induced changes in band gap. It is noteworthy that for zb-InN the LDA gap is actually negative while the real gap is 1.9 eV. The gap in this material is thus almost entirely due to the self-energy correction.

Ionicity explains why the bandgap variation is so much stronger in the III-N series than in the III-As or III-P series. The reason for this is that the high ionicity makes the cation component of the Γ_1^c state relatively more important. The lower ionicity of GaP compared to GaN, for example, is consitent with GaP having an indirect gap. Indeed, the Γ_1^c state having a smaller Ga (heavy element) component is less sensitive to the nuclear potential and lies relatively higher with respect to the Ga_p–P_s like X_1^c state. By the time we get to GaAs, the anion is also a heavier element and thus it also tends to bring the Γ_1^c state down with respect to p-like states. Ionicity also explains why SiC is indirect in both structures while AlN is only direct in wurtzite. The reason is that SiC being less ionic has a relatively smaller component of the Si (i.e. "heavier" element) in the conduction band Γ_1^c state. We note that even for Si, the p-like Γ_{15}^c state lies below the s-like Γ_1

state.

Elastic constants. We have recently also performed full-potential calculations of the zincblende III-nitrides including uniaxial strain distortions. This allowed us to obtain the full set of cubic elastic constants. From the latter, the hexagonal elastic constants can be obtained by a simple tensor transformation operation [60] under the assumption that the bonding is similar in both materials. The changes due to the twinning of the tetrahedrons can be incorporated in this transformation [60].

TABLE 7. Elastic constants for III-nitrides in GPa. (expt. values in parentheses)

		AlN	GaN	InN
	B	202	201	139
cubic	C_{11}	304	296	184
	C_{12}	152	154	116
	C_{44}	199	206	177
hexagonal	C_{11}	398 (345)[a]	396 (296)[b]	271 (190)[b]
	C_{12}	140 (125)	144 (130)	124 (104)
	C_{13}	70 (120)	64 (158)	21 (121)
	C_{33}	468 (395)	476 (267)	375 (182)
	C_{44}	96 (118)	91 (24)	46 (99)

[a] Tsubouchi and Mikoshiba [61]
[b] Savastenko and Sheleg [62]

Table 7 gives our calculated elastic constants for cubic and hexagonal III-nitrides [63]. The deviations from the experimental values are of the order of 20 % for AlN — except for the C_{13} which is difficult to measure — and worse for the other two materials. Particularly disturbing is the deviation by almost a factor 2 for the C_{11} and C_{33} in GaN and InN. These large elastic constants are closely related to the Youngs moduli in the c-plane and perpendicular to it and should be more easy to determine than the shear moduli. These discrepancies are much worse than typical for LDA results and suggest problems with the experimental values. We note that for Si [19], Diamond [19], and SiC [45], the elastic constants obtained by this method are to within 10 % of the experimental values. Only for AlN are the experimental values given here based on sound velocity measurements. In the other cases, they are based on analyses of X-ray linewdiths in powders, which is a rather indirect and probably inaccurate method for obtaining

elastic constants. The poor quality and small sizes of crystals available at the time of the measurements is probably responsible for these experimental problems.

Ga3d and In4d semicore states A noteworthy aspect of the GaN and InN bandstructures is the effects of the Ga3d and In4d semicorelevels. Because the lattice constants of these materials are fairly small, the Ga or In atoms are close to each other and their semicore d states have significant interactions. Also, they are close in energy to the deep N2s states. Indirect interactions through hybridization with N2s thus further broadens these bands. The LDA eigenvalues of Ga3d and In4d actually overlap with the N2s bands. This means that the Ga3d and In4d participate in the bonding. It is found necessary to include these d-states as valence bands in order to obtain accurate values for the ground state properties [16, 23, 64]. On the other hand, in X-ray photoelectron spectroscopy (XPS), the Ga 3d levels are found to be situated well below the N2s. This is another manifestation of the difference between LDA eigenvalues and the true quasiparticle excitations of the system. These effects are more pronounced for narrow bands and increase with increasing energy separation from the Fermi level. We found that the XPS spectrum of Ga3d can be well accounted for by means of the so-called ΔSCF approach [16].

Interfaces We have calculated band-offsets among III-N semiconductors [65, 66]. The calculations were performed for the zincblende crystals and for the {110} interface. Since the valence-band maxima are similar in nature in both strucures, one may expect that valence band offsets would be similar for the wurtzite. We can then obtain the conduction band offsets by adding the experimental gaps.

TABLE 8. Valence-band $\Delta E_v = E_v^B - E_v^A$ (eV) and conduction-band $\Delta E_c = E_c^A - E_c^B$ offsets with ΔE_c^z for zincblende and ΔE_c^w for wurtzite.

	ΔE_v	ΔE_c^z	ΔE_c^w
AlN/GaN	0.85	0.81	1.78
GaN/InN	0.51	1.07	1.09
AlN/InN	1.09	2.15	3.14

The valence-band offset of AlN/GaN measured by XPS [67] is 0.8 ±0.3 eV in good agreement with our results. Interface orientation effects need to be studied separately and are expected to be of the order of a few 0.1 eV.

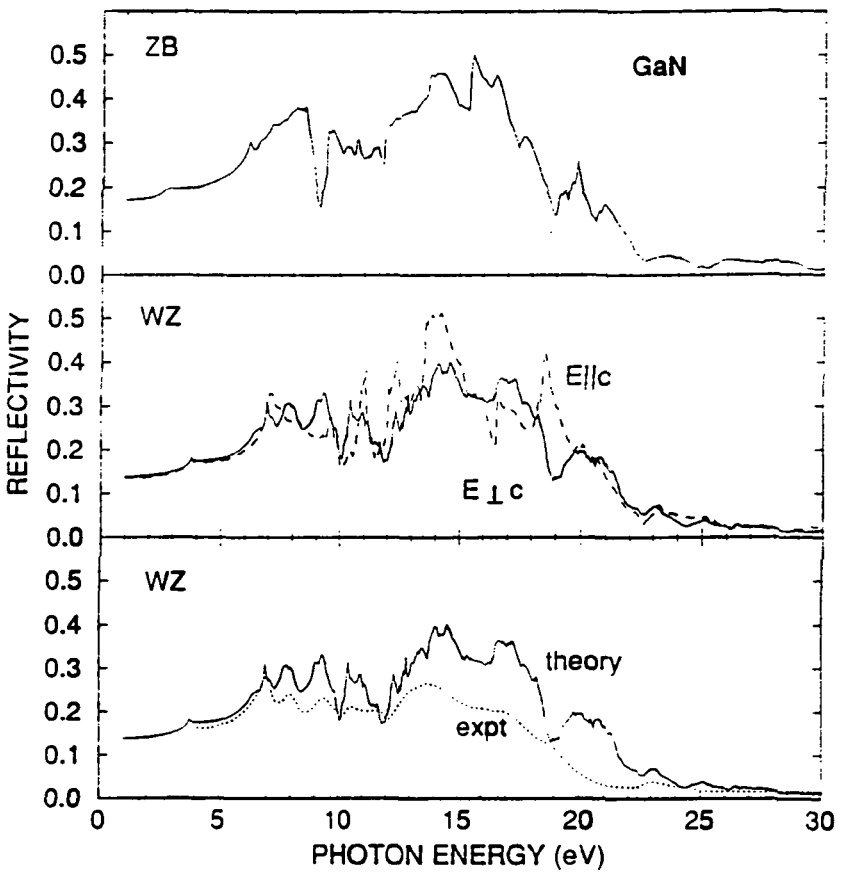

Figure 7. UV-reflectivity of GaN. The bottom panel shows theory and experiment for wurtzite and $E \perp c$; the second panel shows the theoretically predicted polarization dependence for wurtzite: dashed line $E \parallel c$, full line $E \perp c$; the top panel shows the calculated reflectivity for zincblende.

Optical properties We have calculated optical response functions for AlN and GaN. Our results for GaN are shown in Fig. 7. As for SiC polytypes, we find that good agreement with all major peak positions in experimental reflectivity can be achieved with a single constant gap correction or ~1.0

ORIGINAL PAGE IS
OF POOR QUALITY

eV. There is, however, a significant discrepancy in absolute intensity which increases with increasing energy. A possible explanation for this is diffuse scattering in the experiment. Our calculations predict significant differences in spectra between zincblende and wurtzite and significant anisotropy in the case of wurtzite. These remain to be confirmed by experiment. For wurtzite GaN, our calculated results and the experiments by Rife et al. [68], shown here are in good agreement with those of Olson et al. [69]. A more detailed analysis of these spectra will be given elsewhere.

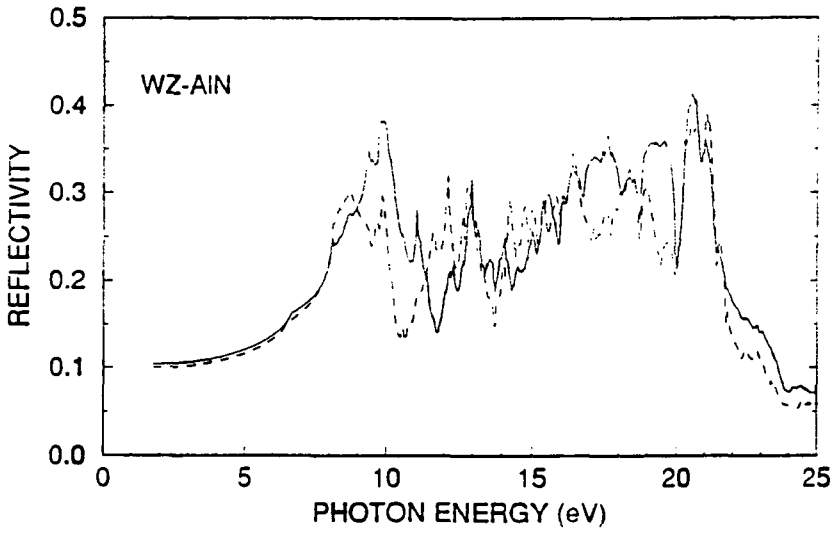

Figure 8. Calculated refletivity of wurtzite AlN: full line. $E \perp c$. dashed line. $E \parallel c$.An LDA gap correction of 1.72 eV was included.

Our calculated reflectivity for wurtzite AlN is shown in Fig. 8. The results are in good agreement with those of Loughin et al. [70] as far as peak positions and general shape of the spectrum is concerned in the energy region below $\sim$ 10 eV. As for GaN, our calculations predict a significantly stronger reflectivity at high energies than observed in the experiment.

4.6. II-IV-N_2 MATERIALS

An interesting class of wide-band-gap semiconductors, which has sofar received very little attention, is formed by the II-IV-V_2 materials. These are derived from the corresponding III-V compound by substituting half of the III elements by a group II and half by a group IV. This does not completely specify the crystal structure. We have performed studies of thes materials

ORIGINAL PAGE IS
OF POOR QUALITY

assuming the chalcopyrite structure because the latter is a simple superstructure of zincblende and is the equilibrium form of II-IV-V_2 materials other than nitrides such as $ZnGeP_2$, $ZnGeAs_2$, $MgSiP_2$. In this structure, each group-V atom is tetrahedrally coordinated with two group-II atoms and two group-IV atoms. We have studied the compounds with II=Be or Mg and IV= Si and C and also $MgSiP_2$ [18]. We have already briefly discussed $BeCN_2$ along with diamond, c-BN and BeO. Among these nitrides, only the silico-nitrides with IV=Si have sofar been synthesized. They have a crystal structure that is derived from wurtzite in a manner similar to how chalcopyrite is derived from zincblende. We have sofar only studied the simpler but related chalcopyrite structure. Our main results are summarized in Table 9.

TABLE 9. Properties of II-IV-V_2 materials: lattice constant a, bond lengths d, bond energy E_b, bulk modulus B, band gap E_g.

	a (Å)	d_{IV-V} (Å)	d_{II-V} (Å)	E_b (eV)	B (GPa)	E_g (eV)
$BeCN_2$	3.71	1.50	1.71	3.8	333	4.62 (6.3)[a]
$MgCN_2$	4.11	1.58	1.92	2.5	210	3.69 (5.0)
$BeSiN_2$	4.10	1.70	1.88	3.0	240	4.47 (5.7)
		1.76[b]	1.76[b]			
$MgSiN_2$	4.44	1.77	2.08	2.8	195	4.03 (5.3)
		1.76[b]	2.08[b]			
$MgSiP_2$	5.64	2.26	2.59	1.9	75	1.77 (2.5)

[a] Including estimated correction, see Petukhov et al. [18]
[b] Experimental values, see Petukhov et al. [18] for original refs.

Generally speaking (except $BeCN_2$), these materials have higher gaps than the corresponding III-nitrides, which is probably related to their higher ionicity. The folding effects of the chalcopyrite lead to conduction-band minima at Γ, except for $MgSiP_2$. Except for $BeCN_2$, however, the valence-band maxima are displaced from Γ. Although the gaps are thus indirect, except in $BeCN_2$, they are very close to the corresponding direct gaps. In Fig. 9 we show the gaps versus lattice constant along with those of the related nitrides, diamond, and BeO. The figure also includes a calculated gap for $AlBN_2$ in the (idealized, i.e. unrelaxed) chalcopyrite structure. The lines are only guides for the eye, and should not be interpreted as gaps of alloys since the latter may exhibit non-linear behavior with lattice constant. One may appreciate from this figure that these materials all have gaps similar to those of diamond and c-BN but extend over a lattice constant range where no binary tetrahedrally bonded compounds occur. They thus fill the gap between the lattice constants of the tetrahedrally bonded

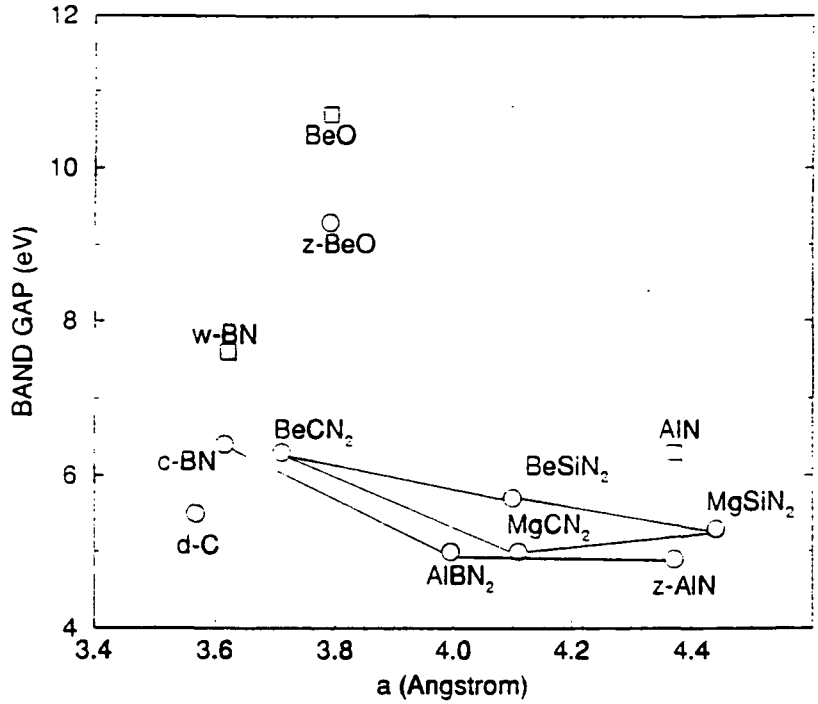

Figure 9. Band gaps of II-IV-N_2 materials and related binary compounds versus effective cubic lattice constant a (Å). The squares indicate wurtzitic compounds, the circles cubic or closely related structures. Note that for BeO and AlN the equilibrium phase is wurtzite while the zincblende phases indicated by $z-$ are hypothetical.

materials made from elements of the second row (B, C, N) only and those made from mixtures of the elements of the second and third row (SiC, BP, AlN). This makes them possibly useful as bufferlayers or substrates for the growth of c-BN and diamond. The figure suggests that even higher gaps can be expected for the corresponding wurtzitic compounds.

An interesting question is whether the carbonitrides which sofar have not been synthesized can be stabilized. From the above cohesive energies and our calculated cohesive energy of SiC and diamond it follows that the reactions

$$MgSiN_2 + 2C \quad - \quad MgCN_2 + SiC, \quad \Delta H = 115\text{kcal/mole} \qquad (5)$$

$$BeSiN_2 + 2C \quad - \quad BeCN_2 + SiC, \quad \Delta H = -84\text{kcal/mole} \qquad (6)$$

are respectively endothermic and exotherimc. The relative unstability of $MgCN_2$ with respect to $MgSiN_2$ follows from its larger mismatch in atomic

radii. Similarly $BeCN_2$ has less strain to overcome than $BeSiN_2$. The synthesis of $BeCN_2$, which is the most interesting of this class of materials because its properties are closest related to those of diamond and because it is a direct gap material in contrat to its parent compound c-BN, would seem to be synthesizable by the substitution of Si by C in the existing compound $BeSiN_2$. It remains an open question whether alternative π-bonded crystal structures are possible for these materials. Their higher ionicity which favors higher coordination, however, disfavors such structures. This has been argued earlier in this paper to be the reason why such structures do not appear for BeO. Since $BeCN_2$ is intermediate in properties between c-BN and BeO, we are presently unable to predict whether it will behave like BN and exhibit π bonding, or whether it will behave like BeO and not show π-bonding.

4.7. ALLOYS

Several alloy systems among the wide-band-gap semiconductors are of interest. The III-nitrides are known to form continuous alloys. Of these, we have sofar only studied the $Ga_xAl_{1-x}N$ system [71].

$Ga_xAl_{1-x}N$ alloys The band gaps were found to behave nearly linearly with concentration and a cross-over takes place between direct and indirect gaps in the zincblende alloys at about 40 % GaN. The relatively low energy of formation ($\Delta E_f \approx 0.02$ eV/atom and hence the good miscibility we found for this alloy system is expected on the basis of the chemical similarity of Al and Ga and the close lattice match.

$Al_xB_{1-x}N$ alloys Alloys with of III-nitrides with c-BN suffer from a much larger atomic size mismatch. We have not yet performed a systematic study of them. Only the 50 % compound with the chalcopyrite structure was investigated in connection with the related II-IV-N_2 compounds. Our calculated cohesive energies for $AlBN_2$, c-BN and AlN yield a formation energy of $\Delta E_f \approx 2$ eV/atom, i.e. two orders of magnitude higher than for $Al_xGa_{1-x}N$. The cohesive energy used here does not include relaxation of the bond lengths and is thus an overestimate. Nevertheless, it is clear that the $Al_xB_{1-x}N$ alloy system will have a much lower solubility. The band gap we obtained for $AlBN_2$ is significantly less than the average of those of z-AlN and c-BN as can be seen in Fig. 9. The bandgap bowing is conventionally described by means of a bowing parameter b defined by

$$E_g(x) = \overline{E}_g + \Delta E_g(x - 1/2) - bx(1 - x), \qquad (7)$$

with $\overline{E}_g = [E_g(0) + E_g(1)]/2$ the average gap and $\Delta E_g = E_g(1) - E_g(0)$ the gap difference between the endpoints A and B. Using our LDA gaps for c-BN, chalcopyrite $AlBN_2$ and z-AlN of respectively 4.73, 3.71 and 3.44 eV, we find $b = 1.5$ eV. Including the estimated gap corrections, we obtain for these numbers respectively: 6.4, 5.0, 4.7, $b = 2.2$ eV. Bond length relaxations are expected to influence this bowing strongly. The present numbers are thus only an indication that bowing is large in this system. A similar situation is expected to hold for $B_xGa_{1-x}N$ alloys.

Heterovalent alloys The heterovalent alloys among group IV compounds, or, elemental solids, and III-V compounds present an even more challenging problem. We have carried out a study of diamond-c-BN alloys [72] and of the alloys of SiC with AlN and BP. All of these are reasonably lattice matched alloys systems. We have thus neglected bond-length relaxations sofar. Details of our calculations for diamond-c-BN were presented in [72]. Our results on the SiC-AlN and SiC-BP were reported at the MRS Spring Meeting 1993 but have not yet been published, except for a brief mention of the SiC-AlN results in [73, 58].

First, we discuss the short-range order in these systems and our computational approach. Because of the donor and acceptor character of IV-V and IV-III bonds respectively, there is a significant energetic advantage in compensating the two types of cation-anion bonds by placing them in close proximity and by incorporating them in equal amounts. Charge transfer from one to the other will satisfy each bond with two electrons and thus yield a gain in band-structure energy [74]. The charging of the bonds that accompanies this, however, leads to a mutual attraction. We thus assume that low-energy configurations have nearest neighbor IV-V and IV-III bonds. For a similar reason, we exclude cation-cation and anion-anion "wrong" bonds completely as these nearest-neighbor interactions would lead to high energies. We are then left with a simple pseudobinary alloy problem in which we consider only disorder on one of the sublattices and place the accompanying anions so as to satisfy the above short-range order charge neutrality or compensation rules. In the case of SiC/BP, it is necessary to take into account the fact that in BP, B behaves as anion and P as cation. Thus we assume Si-P and C-B bonds. The other structures were found to have sufficiently high energies that they could be ruled out [48].

This does not completely specify the relevant local structures but guides the choice of physically plausible structures. We then choose the $L1_2$ ordering for 25 % or 75 % and $L1_0$ ordering for 50 % cation mixtures on the fcc sublattice of the zincblende structure. These form the basis of the so-called Connolly-Williams method [75] in which one considers fcc nearest neighbor tetrahedrons of the type A_nB_{4-n} with A and B the two types of cations and

ORIGINAL PAGE IS
OF POOR QUALITY

n ranging from 0 to 4. Next, we perform first-principles calculations of the total energies and band structures of these mixed ordered compounds. We then assume that the properties of the disordered system can be obtained as a suitable average over these "basis-states". In principle, one should obtain the distribution of clusters in the alloy at a given concentration and temperature by the minimization of the free energy. The latter includes the energy of formation, the configurational entropy, and eventually the vibrational free energy and elastic strain energy contributions. This approach is known as the cluster variation method.

For the alloys considered, we find that the energy of formation is nearly a parabolic function of the concentration and is high. For 50 % SiC-AlN it is about 0.25 eV/atom. This is high and implies that there is only a very limited thermodynamic miscibility. The near parabolicity implies that the Connolly-Williams cluster-expansion model can be mapped onto the ferromagnetic Ising model [72]. This allows as to make an immediate and simple estimate of the miscibility temperature, which is given by $0.816 \times 2\Delta E_f(1/2)/k_B$ with k_B the Boltzman constant and $\Delta E_f(1/2)$ the energy of formation of the 50 % compound. This has a value of ~5000 K in the present case. Lattice relaxation effects and inclusion of longe-range correlations may easily reduce this number by a factor of two. The present calculation thus only gives a rough estimate. The experimental phase diagram [76] of the SiC-AlN alloy system indicates a miscibility temperature of ~2000°C. Furthermore, it indicates that alloys preferentially form in the wurtzite structure except near the SiC rich end where other polytypes are stabilized. In any case, for the present purposes, it suffices to point out that these heterovalent alloys are likely to be metastable towards phase separation up to rather high temperatures. Nevertheless, once they have been formed by non-equilibrium processes, e.g. from a melt or gas phase mixture, the phase separation process may be slow because it would require massive diffusion. The overall conclusion of this is that thermodynamic equilbirum considerations may be rather irrelevant to the actual structure of these alloys. Thus, instead of calculating the thermodynamic equilibrium distributions of the various types of clusters, we can equally well assume a random distribution.

$$P_n = \binom{4}{n} x^n (1-x)^{4-n}, \tag{8}$$

of the 5 types of basic tetrahedron clusters. We use this procedure to obtain a first approximation to the band-gap behavior in the disordered alloys. Before presenting those results, we note that inclusion of configurations of the type we ruled out from the start would drive up the formation energy even higher and reinforce our conclusions. Although such configurations

will probably appear in small amounts due to random errors during growth, they can be considered as defects instead of the average structure. In some sense, they are similar to anitisite defects in a simple binary compound. Our calculations for the interfaces [48] which considered "wrong bonds" of the type Si-Al, C-N, showed that these give rise to defect states in the gap.

Figs. 10 and 11 show our calculated band structures of the ordered compounds of SiC-AlN and SiC-BP respectively. The Brillouin zone notation follows Bradley and Cracknell [77]. Figs. 12 and 13 show the band gaps of the ordered compounds we used as "basis" for the cluster expansion as well as the disordered alloy average obtained using a random probability distribution of the clusters. The bowing coefficients are included in the figure. We give both the LDA values and the corrected gaps for the ordered compounds. We assume here that the correction can be linearly interpolated between the known corrections for the end compounds.

We note that the X^{zb} point where the conduction band-minimum ocurs for SiC and AlN is folded onto Γ in the ordered intermediate compounds. For the 50 % and 75 % AlN compounds, however, the valence-band maximum does not ocur at Γ. This is related to the very flat valence-band maximum along the $\Gamma - X$ direction in the tetragonal $L1_0$ structure which correponds to $\Gamma - M$ in the simple cubic $L1_2$ structure. The valence band maximum in both cases occurs at R. Both the minimum gap and the smallest direct gap are indicated in Fig. 12. The smallest direct gap, in any case is only pseudodirect because it corresponds to a transition form the highest valence state at Γ to the folded X^{zb} minimum. Since the perturbation of the parent band structures is strong in these materials, the matrix elements for these pseudodirect transitions may be appreciable. The curve for the disordered alloy gap is based on the minimum gaps. In SiC-BP, the alloys with 50 % or more BP have negative LDA gaps.

We note that in both cases a very large bowing is present. The bandgaps in SiC-BP are predicted to be smaller than the almost equal gaps at the end points over almost the entire composition range. As in diamond-c-BN, [72] this is related to the type-II offset in this system. Indeed, the band-offset at heterojunctions among these materials is shown in Fig. 14 and indicates that the gap of the overall SiC-BP heterojucntion system is smaller than that of the two pure compounds. This is thus proposed to be the primary cause of the large bowing. SiC-AlN has a type-I offset, i.e. an offset with the larger gap enclosing the smaller gap. Nevertheless, a strong bowing is also apparent here. In both cases the origin of this phenomenon may be argued to be the large charge transfers taking place between the constituent semiconductors. If one thinks of the alloy as a molecular level mixture of regions of BP (or AlN) and SiC, it is clear that charge transfer processes similar to those found at the heterojunction must occur. To what

ORIGINAL PAGE IS
OF POOR QUALITY

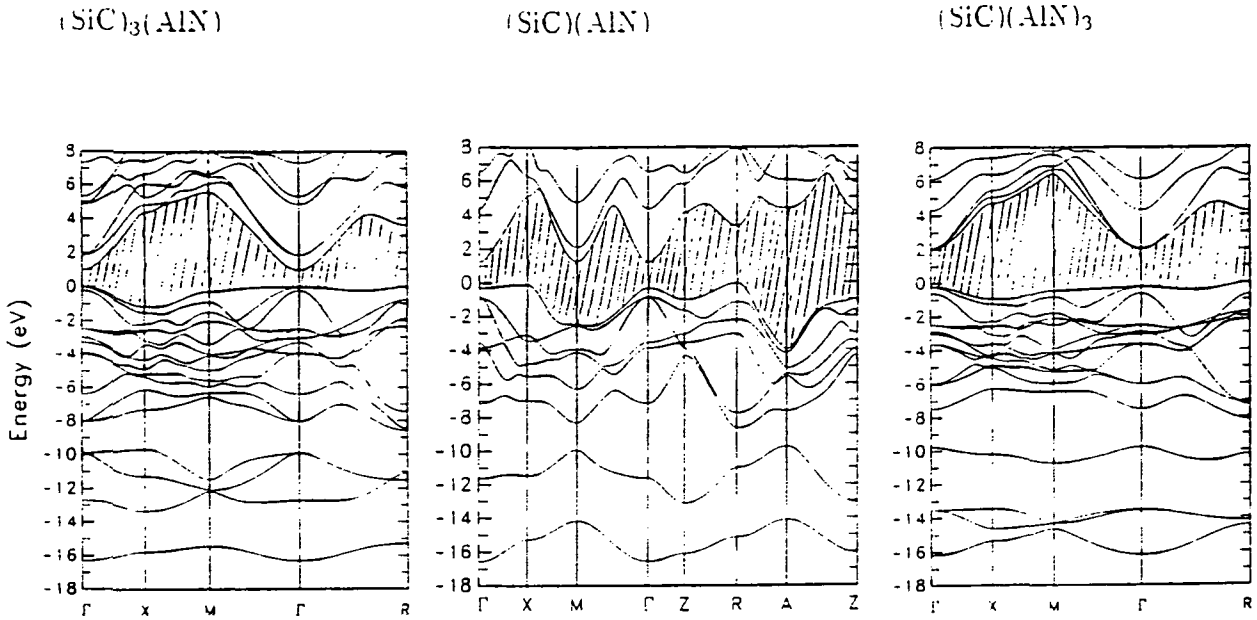

Figure 10. Band structures of ordered compounds of $(SiC)_3(AlN)$, (SiC)(AlN) and $(SiC)(AlN)_3$. The gap is indicated by shading.

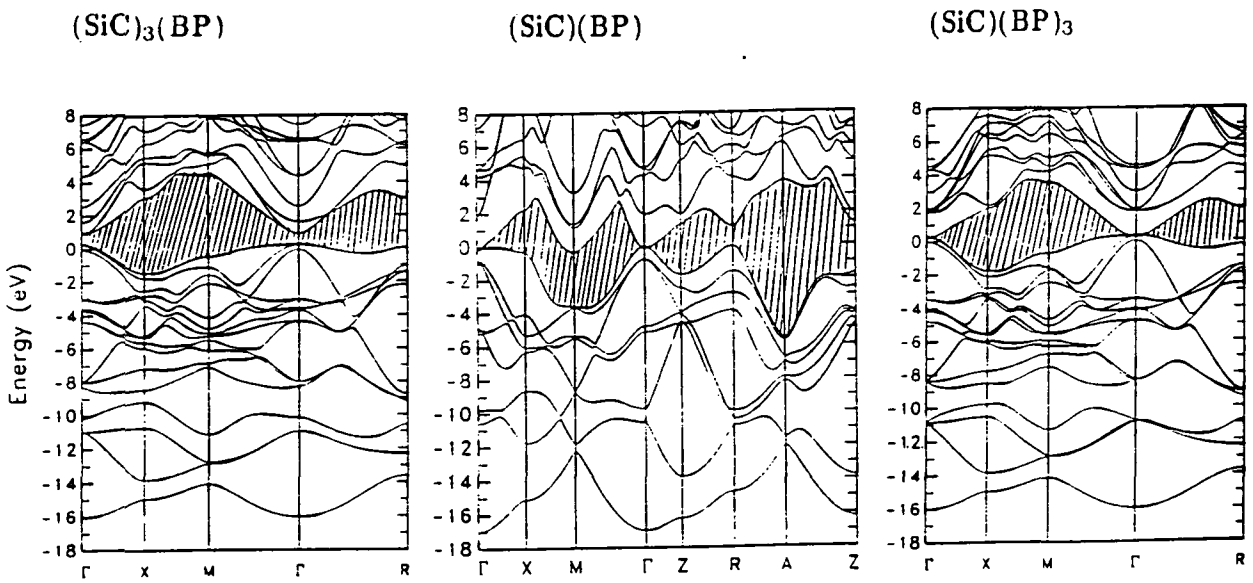

Figure 11. Band structures of ordered compounds of $(SiC)_3(BP)$, (SiC)(BP) and $(SiC)(BP)_3$. The gap is indicated by shading.

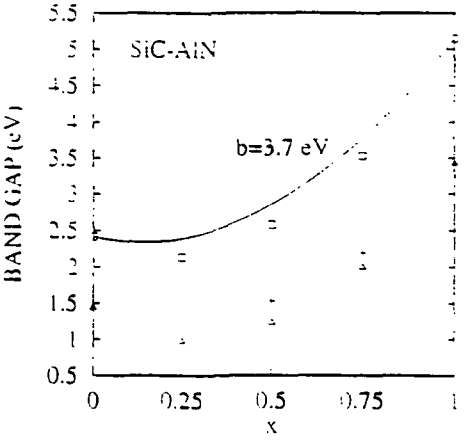

Figure 12. Band gap versus concentration in zincblende $(SiC)_{1-x}(AlN)_x$ alloys: triangles, LDA minimum gaps for ordered compounds: pluses. LDA pseudodirect gaps of the ordered compounds: squares. corrected gaps for the ordered compounds: solid line. corrected gaps for the disordered alloys. b is the bowing parameter.

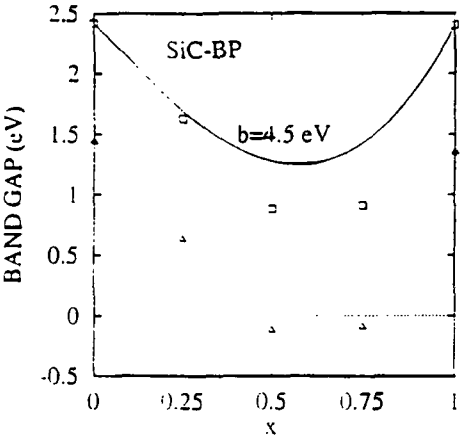

Figure 13. Band gap versus concentration in zincblende $(SiC)_{1-x}(BP)_x$ alloys. triangles. LDA minimum gaps of the ordered compounds: squares. corrected gaps for the ordered compounds: solid line, corrected gap for the disordered alloys. b is the bowing parameter.

extent one can transfer this idea to the homogeneous alloys considered in our calculations is not clear. Qualitatively, however, it is clear that similar B-Si (N-Si) and P-C (C-Al) bonds occur and that the balance between the charge transfers in these bonds determines the electrostatic dipole offsetting the potentials in BP (AlN) units from the ones in SiC units.

We note that for SiC-AlN alloys of wurtzitic structure, a large bowing

ORIGINAL PAGE IS
OF POOR QUALITY

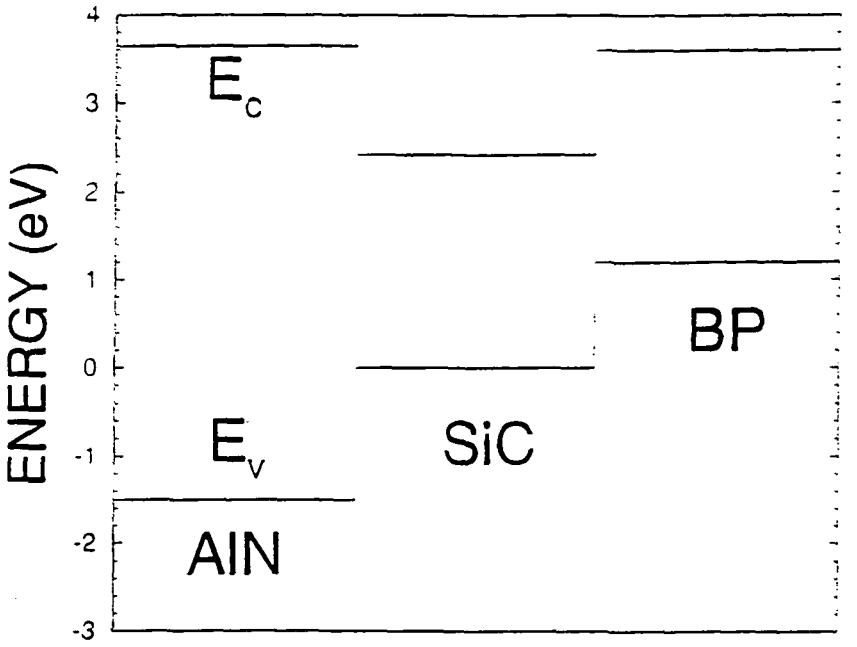

Figure 14. Calculated band offsets at SiC/AlN and SiC/BP zincblende heterojunctions. The valence band maximum E_v of SiC is arbitrarily chosen as zero. If transitivity is assumed the figure also gives an estimate of the AlN/BP offset.

has indeed been found to exist [78] both for the direct $\Gamma - \Gamma$ gap and the indirect $\Gamma - X$ gap. Although our present calculations are for zincblende derived alloys, corresponding charge transfer effects are expected for hte wurtzite alloys. Thus the experimental results provide indirect confirmation of the validity of our results. Work on the wurtzite alloys is in progress.

5. Conclusions

In this paper, we have reviewed the electronic structure and related properties of a wide range of tetrahedrally bonded semiconductors whose common feature is that they include early elements of the periodic table, i.e. Be, B, C, N and O. This survey includes diamond, SiC, the binary compounds of formula III-N with the group-III element including B, Al, Ga, In; the compounds of formula B-V with the group-V element being N, P, and As; and the II-IV-N_2 compounds with IV being Si or C and II being Be and Mg. It also includes the II-VI compound of the second row: BeO. The Be_2C and Be_3N_2 compounds, which have a bonding type that is closely related to tetrahedral bonding, were also included as results for them are relevant

for the discussion of the synthesis of $BeCN_2$. Bandgaps, lattice constants, bond energies or cohesive energies, bulk moduli and, in the case of the nitrides, other elastic constants were presented. The strong covalent bonding and the deep N2p levels were shown to be the basic reason for the wide band gaps occuring in these materials. The interrelationship between various properties, and, in particular, between crystal structure and electronic structure was discussed in detail. Special attention was given to SiC which forms in a large number of polytypes. The optical reflectivity of some of the most important polytypes of SiC and of GaN and AlN were discussed. They provide an important experimental check of the calculated band structures. We have revealed the trends with atomic number and ionicity. Related issues such as the electronic structure of alloys and interfaces were discussed. Besides an extensive discussion of previously published material, the paper includes new results on SiC-BP and SiC-AlN alloys, new results on hexagonal modifications of diamond, BN and BeO, and on the related material Be_2C. We have analyzed the prospects for synthesis of a new matrial $BeCN_2$ on the basis of our calculated energies of formation.

Acknowledgements

We thank M. Alouani, M. van Schilfgaarde and M. Methfessel for providing computer programs, J. C. Angus, A. Argoitia for collaborations on diamond, W. J. Choyke and R. P. Devaty and coworkers for collaborations on SiC reflectivity, and J. Rife, W. R. Hunter and D. K. Wickenden for collaborations on GaN reflectivity. The nitride work was supported by NSF DMR-92-22387, the diamond work by the NSF-MRG DMR-89-03527 and ONR N-00014-89-J-1631 and the SiC work by Wright-Laboratories (Contract No. F33615-93-C-5347) and NASA Lewis Research Center (NCC 3-25). Part of the computations were done a the Ohio Supercomputer Center.

References

1. J. C. Phillips, *Bonds and Bands in Semiconductors*, (Academic, New York, 1973).
2. W. A. Harrison, *Electronic Structure and Properties of Solids*, (Dover, New York 1989).
3. W. R. L. Lambrecht and B. Segall, *Phys. Rev. B* **41**, 2832 (1990).
4. R. M. Wentzcovitch, A. Continenza, and A. J. Freeman, in *Diamond, Silicon Carbide and Related Wide Bandgap Semiconductors*, ed. J. T. Glass, R. Messier, and N. Fujimori, Mater. Res. Soc. Symp. Proc. Vol. 162, (MRS, Pittsburgh 1990), p. 611.
5. C.-Y. Yeh, Z. W. Lu, S. Froyen and A. Zunger *Phys. Rev. B* **46**, 10086 (1992).
6. H. Amano, M. Kito, K. Hiramatsu, *Jpn. J. Appl. Phys.* **28**, L2112 (1989).
7. R. H. Wentorf, Jr., *J. Chem. Phys.* **26**, 956 (1957); *ibid.* **34**, 809 (1961); *ibid.* **36**, 1990 (1962).
8. P. Hohenberg and W. Kohn, *Phys. Rev.* **136**, B864 (1964); W. Kohn and L. J. Sham *ibid.* **140**, A1133 (1965).
9. L. Hedin and B. I. Lundqvist, *J. Phys. C* **4**, 2064 (1971).

10. L. Hedin, *Phys. Rev.* **139**, A796, (1965).
11. M. S. Hybertsen and S. G. Louie, *Phys. Rev. B* **34**, 5390 (1986).
12. R. W. Godby, M. Schlüter, and L. J. Sham, *Phys. Rev. B* **37**, 10159 (1988).
13. M. Rohlfing, P. Krüger, and J. Pollmann, *Phys. Rev. B* **48**, 17791 (1993).
14. M. Palummo, L. Reining, R. W. Godby, and C. M. Bertoni in *Proc. 21 st Int. Conf. on the Physics of Semiconductors*, held in Beijing, Aug. 1992, ed. Ping Jiang, and Hou-Zhi Zheng, (World Scientific, Singapore 1993), p. 89.
15. F. Bechstedt and R. Del Sole, *Phys. Rev. B* **38**, 7710 (1988).
16. W. R. L. Lambrecht, S. Strite, G. Martin, A. Agarwal, H. Morkoç, and A. Rockett, *Phys. Rev. B* (1994), submitted.
17. O. K. Andersen, *Phys. Rev. B* **123**060 (1975); O. K. Andersen, O. Jepsen, and M. Šob, in *Electronic Band Structure and its Applications*, edited by M. Yussouff, (Springer, Heidelberg, 1987).
18. A. G. Petukhov, W. R. L. Lambrecht and B. Segall, *Phys. Rev. B* **49**, 4549 (1993).
19. M. Methfessel, *Phys. Rev. B* **38**, 1537 (1988); M. Methfessel, C. O. Rodriguez, and O. K. Andersen, *Phys. Rev. B* **40**, 2009 (1989); H. M. Polatoglou and M. Methfessel, *ibid.* **41**, 5898 (1990).
20. W. R. L. Lambrecht and B. Segall, *Phys. Rev. B* **40**, 9909 (1989); **41**, 5409 (1990).
21. M. R. Salehpour and S. Satpathy, *Phys. Rev. B* **41**, 3048 (1990).
22. I. Gorczyca and N. E. Christensen, *Physica B* **185**, 410 (1993).
23. W. R. L. Lambrecht and B. Segall, in *Wide Band Gap Semiconductors*, ed. T. D. Moustakas, J. I. Pankove, and Y. Hamakawa, Mater. Res. Soc. Symp. Proc. Vol. **242** (MRS, Pittsburg, 1992) p. 367.
24. W. R. L. Lambrecht in *Diamond, Silicon Carbide and Nitride Wide-Bandgap Semiconductors*, ed. C. H. Carter, Jr., G. Gildenblat, S. Nakamura, and R. J. Nemanich, Mater. Res. Soc. Symp. Proc. Vol. 339 (1994), to be published.
25. K. J. Chang, S. Froyen, and M. L. Cohen, *J. Phys. C* **16**, 3475 (1983); K. J. Chang and M. L. Cohen, *Solid State Commun.* **50**, 487 (1984).
26. W. R. L. Lambrecht and B. Segall, *Phys. Rev. B* **45**, 1485 (1992).
27. B. F. Levine, *Phys.Rev. B* **7**, 2600 (1973).
28. S. Fahy, S. G. Louie, and M. L. Cohen, *Phys. Rev. B* **34**, 1192 (1986); *ibid.* **35**, 7623 (1987).
29. R. Wentzcovitch, S. Fahy, M. L. Cohen, and S. G. Louie, *Phys. Rev. B* **38**, 6191 (1988).
30. S. P. Mehandru, A. B. Anderson, and J. C. Angus, *J. Phys. Chem.* **96**, 10978 (1992).
31. W. R. L. Lambrecht, C. H. Lee, B. Segall, J. C. Angus, Z. Li, and M. Sunkara, *Nature* **364**, 607 (1993).
32. J. Tersoff, *Phys. Rev. Lett.* **61**, 2879 (1988).
33. W. R. L. Lambrecht and B. Segall, *J. Mater. Res.* **7**, 696 (1992).
34. W. R. L. Lambrecht, *Physica B* **185**, 512 (1993).
35. S. Koizumi, T. Murakami, T. Inuzuka, and K. Suzuki, *Appl. Phys. Lett.* **57**, 563 (1990).
36. A. Argoitia, J. C. Angus, J. S. Ma, L. Wang, P. Pirouz, and W. R. L. Lambrecht, *J. Mater. Res.* (1994), in press; L. Wang, P. Pirouz, A. Argoitia, J. S. Ma, and J. C. Angus, *Appl. Phys. Lett.* **63** 1336 (1993).
37. A. Argoitia, J. C. Angus, L. Wang, X. I. Ning, and P. Pirouz, *J. Appl. Phys.*, **73**, 4305 (1993).
38. C. H. Lee, W. R. L. Lambrecht, and B. Segall, unpublished.
39. R. O. Jones and O. Gunnarsson, *Rev. Mod. Phys.* **61**, 689 (1989).
40. A. R. Verma and P. Krishna, *Polymorphism and Polytypism in Crystals*, (Wiley, New York, 1966).
41. G. S. Zhdanov, *C. R. Acad. SCi. USSR*, **48**, 43 (1945).
42. V. Heine, C. Cheng, G. E. Engel, and R. J. Needs, in *Wide Band Gap Semicondcutors*, edited by T. D. Moustakas, J. I. Pankove, Y. Hamakawa, Mater. Res. Soc. Symp.

Proc. Vol. 242 (MRS, Pittsburgh, 1992) p. 507; C. Cheng, R. J. Needs, and V. Heine, *J. Phys. C* **21**, 1049 (1988); J. J. A. Shaw and V. Heine, *J. Phys.: Condens. Matter* **2** 4351 (1990); C. Cheng, V. Heine and I. L. Jones, *ibid.*, 5097; C. Cheng, V. Heine and R. J. Needs, *ibid.* 5115. N. Churcher, K. Kunc, and V. Heine, *J. Phys. C* **19**, 4413 (1986).

43. P. Pirouz, *Scripta Met.* **23**, 401 (1989); P. Pirouz and J. W. Wang, *Ultramicroscopy* **51**, 189 (1993); P. Pirouz, *Inst. of Physics Conf. Ser.* No. 104, p. 49 (1989).
44. J. Pezoldt, A. A. Kalnin, D. R. Moskwina, and W. D. Savelyev, *Nucl. Instr. and Meth. in Physics Res.*, **B80/81**, 943 (1993). A. A. Kalnin, F. Neubert, J. Pezoldt, in *Proc. 4th European Conference on Diamond, Diamond-like and Related Materials, Albufeira, Portugal, Sepember 20-24, 1993*, ed. P. K. Bachman, I. M. Buckley-Golder, J. T. Glass, M. Kamo, (Elsevier Sequoia, Lausanne 1994), p. 346; also published in *Diamond and Related Materials* Vol. 3, Nos.4–6.
45. W. R. L. Lambrecht, B. Segall, M. Methfessel, and M. van Schilfgaarde, *Phys. Rev. B* **44**, 3685 (1991).
46. W. R. L. Lambrecht, B. Segall, W. Suttrop, M. Yonagathan, R. P. Devaty, W. J. Choyke, J. A. Edmond, J. A. Powell, and M. Alouani, *Appl. Phys. Lett.* **63**, 2747 (1993); and unpublished.
47. W. J. Schaffer, G. H. Negley, K. G. Irvine, and J. W. Palmour, in *Diamond, Silicon Carbide and Nitride Wide-Bandgap Semiconductors*, ed. C. H. Carter, Jr., G. Gildenblat, S. Nakamura, and R. J. Nemanich, Mater. Res. Soc. Symp. Proc. Vol. 339 (1994), to be published.
48. W. R. L. Lambrecht and B. Segall, *Phys. Rev. B* **43** 7070 (1991).
49. W. R. L. Lambrecht and B. Segall, *Acta metal. mater.* **40**, S17 (1992).
50. W. R. L. Lambrecht and B. Segall, *Phys. Rev. B* **41**, 8353 (1991); *ibid.* **42**, 1462 (1990); W. R. L. Lambrecht, C. H. Lee and B. Segall, in *Atomic Scale Structure of Interfaces*, edited by R. D. Bringans, R. M. Feenstra and J. M. Gibson, Mater. Res. Soc. Symp. Proc., Vol. 159 (MRS, Pittsburgh 1990), p. 377-82; W. R. L. Lambrecht, C. H. Lee, M. Methfessel, M. van Schilfgaarde, C. Amador, B. Segall, in *Defects in Materials*, Mater. Res. Soc. Symp. Proc.,Vol. 209, edited by P. D. Bristowe, J. E. Epperson, J. E. Griffith and Z. Liliental-Weber, (MRS, Pittsburgh 1991), p. 667.
51. R. M. Wentzcovitch, K. J. Chang, and M. L. Cohen, *Phys. rev. B* **34**, 1071 (1986).
52. R. M. Wentzcovitch, and M. L. Cohen, *J. Phys. C* **19**, 6791 (1986).
53. *Landolt-Börnstein: Numerical Data and Functional Relationships in Science and Technology*, New Series, Group III, Vol. 17a, edited by O. Madelung, (Springer, Berlin 1982).
54. A. Muñoz and K. Kunc, *Physica B* **185**, 422, (1993).
55. P. Perlin, C. Jauberthie-Carillon, J. P. Ithie, A. San Miguel, I. Grzegory, and A. Polian, *Phys. Rev. B* **45**, 83 (1992).
56. H. Volstädt, E. Ito, M. Akaishi, S. Akimoto, and O. Fukunara, *Proc. Jpn. Acad. B* **66** 7 (1991).
57. M. Ueno, M. Yoshida, A. Onodera, O. Shimomura, and K. Takemura, in *Proc. 5th Int. Conf. High pressure in Semiconductor Physics*, Kyoto (1992), *Jpn. J. Appl. Phys.* **32**, Suppl. 32-1, 42 (1993).
58. W. R. L. Lambrecht and B. Segall, in *Properties of the Group-III Nitrides*, edited by J. H. Edgar, EMIS Data Review Series, (IEE, Stevenage Herts, UK 1994), in press.
59. W. R. L. Lambrecht, B. Segall, and O. K. Andersen, *Phys. Rev. B* **41**, 2813 (1990).
60. R. M. Martin, *Phys. Rev. B* **6**, 4546 (1972).
61. K. Tsubouchi and N. Mikoshiba, *IEEE Trans. Sonics Ultrason.* **SU-32**, 634 (1985).
62. V. A. Savastenko and A. U. Sheleg, *Phys. Stat. Sol. (a)* **48** K135 (1978); A. U. Sheleg and V. A. Savastenko, *Inorg. Mater.* **15** 1257 (1979).
63. K. Kim, W. R. L. Lambrecht, and B. Segall, *Phys. Rev. B* (1994), in press.
64. V. Fiorentini, M. Methfessel, and M. Scheffler, *Phys. Rev. B* **47**, 13353 (1993).
65. E. A. Albanesi, W. R. L. Lambrecht, and B. Segall, *J. Vac. Sci. Technol. B* (1994), in press (PCSI-21 Proceedings).

66. E. A. Albanesi, W. R. L. Lambrecht, and B. Segall, in *Diamond, Silicon Carbide and Nitride Wide-Bandgap Semiconductors*, ed. C. H. Carter, Jr., G. Gildenblat, S. Nakamura, and R. J. Nemanich, Mater. Res. Soc. Symp. Proc. Vol. 339 (1994), to be published.
67. G. Martin, S. Strite, A. Botchkarev, A. S. Agarwal, A. Rockett, W. R. L. Lambrecht, B. Segall, and H. Morkoç, *Appl. Phys. Lett.*, (1994), to be published.
68. J. Rife, W. R. Hunter, W. R. L. Lambrecht, B. Segall, and D. K. Wickenden, *Bull. Am. Phys. Soc*, **39**, 211 (1994); and unpublished.
69. C. G. Olson, D. W. Lynch, and A. Zehe, *Phys. Rev. B* **24**, 4629 (1981).
70. S. Loughin, R. H. French, W. Y. Ching, Y. N. Xu, and G. A. Slack, *Appl. Phys. Lett.* **63**, 1182 (1993); and S. Loughin, Ph. D. Thesis, Univ. of Pennsylvania, Philadelphia 1992.
71. E. A. Albanesi, W. R. L. Lambrecht, B. Segall, *Phys. Rev. B* **48**, 17841 (1993).
72. W. R. L. Lambrecht and B. Segall, *Phys. Rev. B* **47** , 9289 (1993)
73. W. R. L. Lambrecht, E. A. Albanesi, and B. Segall, in *Proc. International Conference on Silicon Carbide and Related Materials*, Washington DC, November 1993, in press.
74. W. R. L. Lambrecht, C. Amador, and B. Segall, *Phys. Rev. Lett.* **68**, 1363 (1992).
75. J. W. D. Connolly and A. R. Williams, *Phys. Rev. B* **27**, 5169 (1983).
76. A. Zangvil and R. Ruh, *J. Am. Ceram. Soc.* **71**, 884 (1988).
77. W. C. Bradley and A. P. Cracknell, *The Mathematical theory of Symmetry in Solids: Representation Theory for Point Groups and Space Groups* (Clarendon Press, Oxford 1972).
78. G. K. Safaraliev, Yu M. Tairov, and V. F. Tsvetkov, *Sov. Phys. Semicond.* **25**, 865 (1991).

Ref. 6

Theoretical Study of the Electronic, Optical, Interface, and Alloy Properties of SiC and the Group-III-Nitrides

W R L Lambrecht, E A Albanesi, and B Segall

Department of Physics, Case Western Reserve University, Cleveland, OH-44106-7079

ABSTRACT: We present a brief overview of the electronic structure studies of SiC and the III-nitrides performed or in progress in our group. The trends in the band structure across the series and the dependence on polytype are discussed as well as the relation between band-offsets at interfaces and band-gap bowing.

1. INTRODUCTION

SiC and the Group-III Nitrides form a closely related class of wide-band-gap semiconductors. Here we present a brief overview of their electronic structure and related properties. This paper is mainly meant as a guide to previous and on-going work carried out in our group. A full account has been or will be presented elsewhere. Details of the computational approach can be found in the references. Briefly, we use the linear muffin-tin orbital (LMTO) method (see Andersen *et al.* 1987 for a recent description) combined with local density functional theory. Most of our work used the atomic-sphere-approximation (ASA). The full-potential version (FP-LMTO) was used in some cases as indicated.

2. BULK ELECTRONIC STRUCTURE

We have calculated the electronic band structure for SiC, BN, AlN, GaN, and InN in both the zincblende (zb) and wurtzite (wz) structures (Lambrecht and Segall 1992, 1993a). The minimum band gaps at the experimental lattice constant are summarized in Table I.

Table I: Calculated minimum band gaps for wurtzite and zincblende SiC and group-III-nitrides with experimental values in parentheses (in eV). The numbers in square brackets are obtained from FP-LMTO, others within ASA.

		E_G^{zb}		E_G^{wz}
SiC	$\Gamma_{15} - X_1$	1.4 (2.417)[a]	$\Gamma_6 - M_1$	2.7 [2.6]
			$\Gamma_6 - K_2$	2.8 [2.2] (3.30)[b]
BN	$\Gamma_{15} - X_1$	4.3 (6.4)[c]	$\Gamma_6 - K_2$	5.7
AlN	$\Gamma_{15} - X_1$	3.4	$\Gamma_1 - \Gamma_1$	4.6 (6.28)[d]
GaN	$\Gamma_{15} - \Gamma_1$	2.0 (3.5)[e]	$\Gamma_1 - \Gamma_1$	2.4 (3.6)[f]
InN	$\Gamma_{15} - \Gamma_1$	$\approx$0.1	$\Gamma_6 - \Gamma_1$	0.3 (2.05)[g]

[a] Humphreys R G, Bimberg D, and Choyke W J 1981, *Solid State Commun.* **39** 163

[b] Patrick L, Hamilton D R, and Choyke W J 1966, *Phys. Rev.* **143** 526

[c] Chrenko R M 1974, *Solid State Commun.* **14** 511

[d] P. B. Perry and R. F. Rutz 1978, Appl. Phys. Lett. **33**, 39

[e] Strite S, Ruan J, Li Z, Salvador A, Chen H, Smith D J, Choyke W J, and Morkoc H 1990, *J. Vac. Sci. Technol. B* **9** 192

[f] Dingle R, Sell D D, Stokowski S E, Dean P J, and Zetterstorm R B 1971, *Phys. Rev. B* **3** 497

[g] Tyagai V A, Evstigneev A M, Krasiko A N, Andreeva A F, and Malakhov V Ya 1977, *Sov. Phys. Semicond.* **11** 1257

The ASA-LMTO calculated equilibrium lattice volumes, cohesive energies, bulk moduli and their pressure derivatives for zb and wz SiC, AlN, GaN and zb-BN were reported by

ORIGINAL PAGE IS
OF POOR QUALITY

Lambrecht and Segall (1992,1989) and agree well with Gorczyca and Christensen (1993) and other calculations referenced there.

We note that the local density approximation (LDA) underestimates the gap by 1–2 eV in these systems, in agreement with simple estimates of the self-energy correction introduced by Bechstedt and Del Sole (1988) and applied to these materials by Lambrecht and Segall (1992). From our calculations of optical reflectance discussed below, the correction is found to be nearly a constant shift of the conduction bands and to be independent of polytype. For 2H-SiC, we note that the gaps at K and M are very close within ASA while FP-LMTO correctly gives the minimum gap to be at K. The K_{2c} state must thus be particularly sensitive to non-spherical contributions to the potential. Similar FP corrections are thus expected for the nitrides but do not change the conclusions about the location of the minimum bandgap.

Althought the different polytypes have nearly the same total energies, they have quite different band structures, including different gaps and different locations of the conduction-band minima. The origin of these changes was explained by Lambrecht and Segall (1992) by comparing the band structures of ZB and WZ in the same Brillouin zone (BZ). The conduction band-minima at K_{ZB} (X_h) move up in the zincblende (wurtzite) structure. This is due to the fact that K_{WZ} (X_h) has lower symmetry in the zincblende (wurtzite) structure. These effects change the location of the conduction band minimum in BN, AlN, and SiC but not in GaN and InN, because in the latter, the minimum always stays at Γ as a result of the deeper potential for cation-s orbitals for the higher Z-elements.

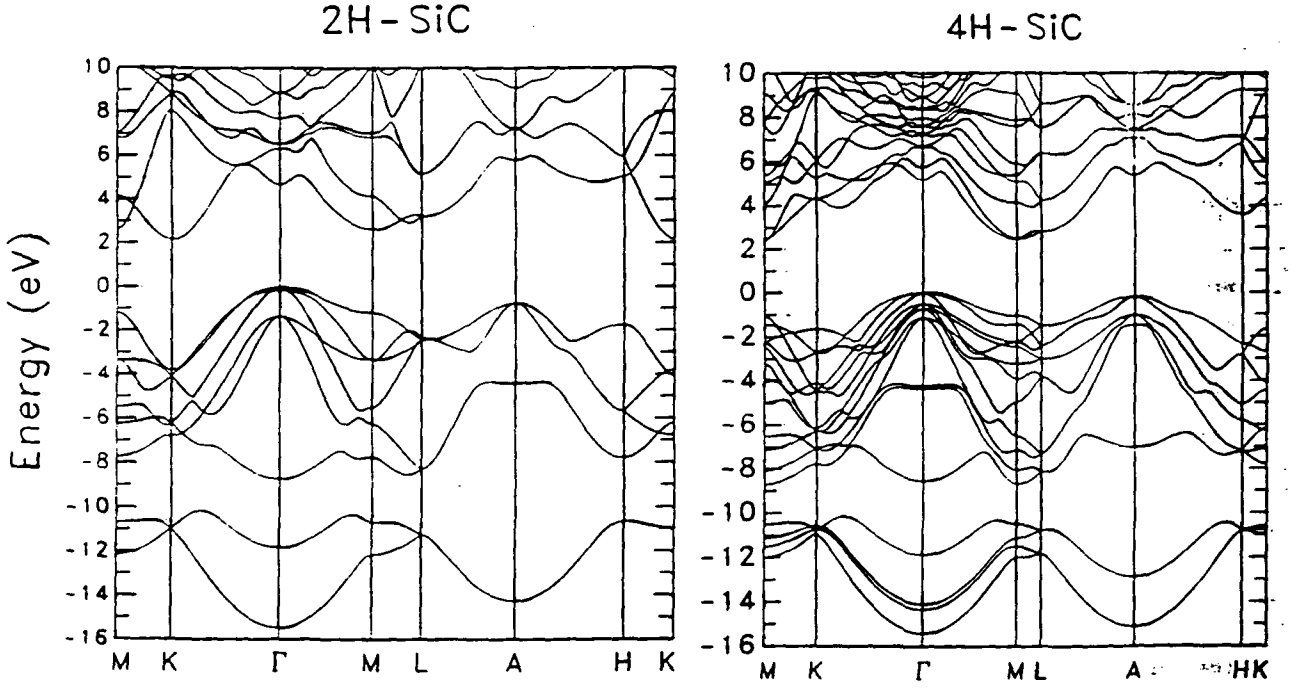

Figure 1: Band structure of 2H and 4H SiC.

The band-structure of the intermediate 4H polytype can be understood in terms of folding effects of the 2H band structure. The band structures of 2H (using FP) and 4H SiC (using ASA) are shown in Fig. 1. The bands on the surface of the 2H-BZ ($L - A - H$) are doubly degenerate in 2H because of the presence of a six-fold screw axis along c. These bands are *essentially folded onto the $M - \Gamma - K$ plane of the 4H BZ, the degeneracy being lifted in the* lower symmetry 4H structure. The bands now become doubly degerenate on the 4H $L - A - H$ plane corresponding to the six-fold screw axis with double pitch.

The optical response functions ($\epsilon_2(\omega)$, $\epsilon_1(\omega)$, and the reflectance) have been calculated using

ORIGINAL PAGE IS
OF POOR QUALITY

the muffin-tin orbital basis set for 3C, 2H and 4H SiC. The results for 3C and 4H SiC were presented in (Lambrecht *et al.* 1993b) and (Suttrop *et al.* 1993). Satisfactory agreement between theory and experiment is obtained for the major peak positions of 3C and 4H up to 10 eV including a constant LDA correction. Preliminary results on the nitrides indicate a similar conclusion.

3. STRAIN EFFECTS

A separate investigation using the FP-LMTO method was made of the strain effects on the band-structure of 3C-SiC (Lambrecht *et al.* 1991a). This study included a calculation of the full set of elastic constants. The elastic constants tensor is only weakly dependent on the polytype. Hence, those for one polytype can be obtained (approximately) from those for another by an appropriate coordinate transformation. We thus obtained good agreement with experimental data for the elastic constants of hexagonal or α-SiC, no distinction being made here between the various hexagonal polytypes.

The strain effects on the band-structure were reported in the form of deformation potentials (Lambrecht *et al.* 1991a). The important deformation potentials, in Pikus and Bir's notation and in eV, for the band gap edges are

Γ_{15}^{v}	a^{v}	b^{v}	d^{v}	d_s	X_{1c}^{c}	Ξ
	1.3	−2.1	−6.0	21.5		8.9

To our knowledge the only deformation potential for which there are experimental data available is the acoustic deformation potential Ξ for the conduction band minimum at X. It was determined to be 22 eV by analyzing the width of cylcotron resonance lines as a function of temperature and assuming a $\tau \propto T^{-3/2}$ behavior (Kaplan *et al.* 1985). The range of the data, however, is too narrow to determine this behavior unambiguously. An alternative (and even better) fit to the data, shown in Fig. 2, is obtained if we assume that in addition to the deformation potential scattering, there is a significant impurity scattering, increasing with increasing temperature and approximately described by an inverse lifetime $\tau_i^{-1} = 1.3(T - 26)10^{10}s^{-1}$. At present, we do not have a well developed theory for the linear dependence of the impurity scattering contribution. However, an increasing τ_i^{-1} with increasing temperature would be expected for scattering from neutral impurity complexes, a situation which is expected for highly compensated material and likely to be the case in SiC samples available at that time. We note that Kaplan et al. (1993) reported a new value of 12.6 eV for the deformation potential for samples of higher quality.

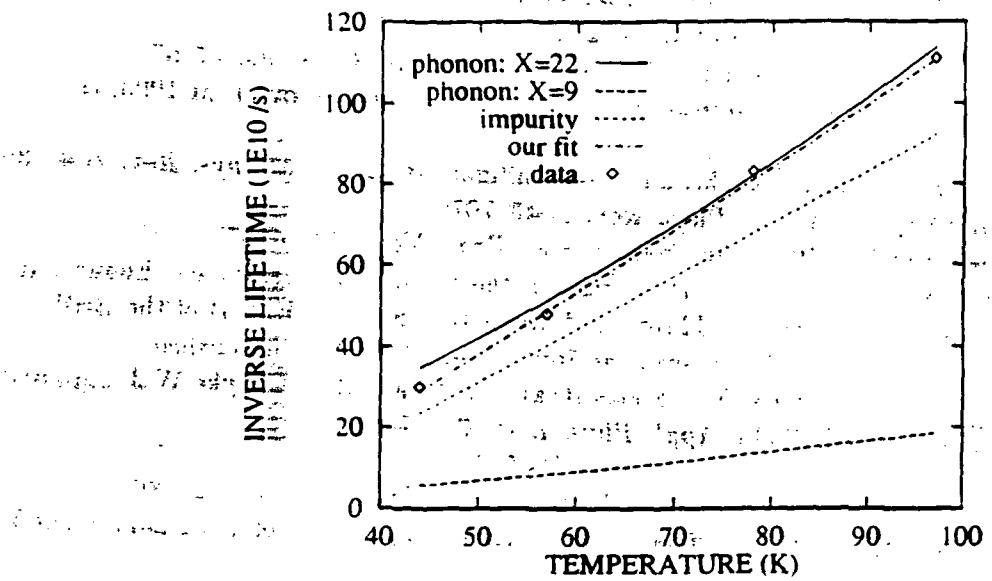

Figure 2: Fits of the inverse lifetime, see text.

ORIGINAL PAGE IS
OF POOR QUALITY

4. HETEROJUNCTIONS AND ALLOYS

The electronic structure of alloys was studied using the cluster-expansion approach as described by Lambrecht and Segall (1993c) The valence-band offsets have been determined for SiC/AlN and SiC/BP {110} heterojunctions (Lambrecht and Segall 1991b) to be 1.5 and 1.2 eV respectively. For SiC/BP the offset is of type II (staggered). In that case, the effective gap of the system is smaller than the smaller of the two. Consequently, a large bowing is expected for the alloy. Indeed, we find a bowing parameter $b = 4.4$ eV, with b defined by

$$E_G(x) = \overline{E}_G + \Delta E_G(x - 1/2) - bx(1 - x). \quad (1)$$

where $\overline{E}_G = [E_G(0) + E_G(1)]/2$ is the average gap and $\Delta E_G = E_G(1) - E_G(0)$ is the gap difference between the endpoints. Even for SiC/AlN, however, we find a large bowing of 3.1 eV. For SiC/AlN, experimental data were reported for the 2H-polytype (Safaraliev *et al.* 1991). In qualitative agreement with our calculations for zincblende, a large bowing of 5.2 eV was obtained for the indirect minimum bandgap $\Gamma - X$ as well as for the direct $\Gamma - \Gamma$ band gap ($b = 4.4$ eV.) One may speculate that the large bowing for SiC/AlN and SiC/BP is related to the heterovalent nature of these alloys which leads to important charge re-arrangements and hence a large dipole at the heterojunctions and large deviations from a "virtual crystal" picture with averaged cations and anions in the alloy.

We also studied the band-gap bowing in zincblende $Al_xGa_{1-x}N$ alloys (Albanesi *et al.* 1993). In that case, we determined the cross-over from direct to indirect band gap to take place at $x \approx 0.6$. The band-gap bowing coefficient in this system was found to be negligibly small and slightly upward (i.e. $b < 0$) if bond-length relaxations are included. For the direct gap $\Gamma_{15c} - \Gamma_{1c}$ the nearly linear behavior is in qualitative agreement with the experimental data for the wurtzite $\Gamma_{1c} - \Gamma_{1c}$ gap, which is expected to behave similarly.

Acknowledgement: We acknowledge support from NSF, ONR and NASA Lewis Research Center during various stages of this work. E A Albanesi acknowledges support from CONICET (Argentina).

REFERENCES:

Albanesi E A , Lambrecht W R L and Segall B 1993. *Phys. Rev. B*, in press

Andersen O K, Jepsen O, and Šob M 1987. *Electronic Band Structure and its Applications*, ed. Yussouff M. (Springer, Heidelberg) p 1

Bechstedt F and Del Sole R 1988. *Phys. Rev. B* **38** 7710

Gorczyca I and Christensen N E 1993. *Physica B* **185** 410

Kaplan R, Wagner R J, Kim H J , and Davis R J 1985. *Solid State Commun.* **55** 67

Kaplan R, Moore W J, Freitas J A , Altaiskii Yu M, Zuev V L, and Ivanova L M 1993, this Conf. Proc.

Lambrecht W R L and Segall B 1989, *Phys. Rev. B* **40** 9909

Lambrecht W R L, Segall B, Methfessel M, and van Schilfgaarde M 1991a, *Phys. Rev. B* **44** 3685

Lambrecht W R L and Segall B 1991b, *Phys. Rev. B* **43** 7070

Lambrecht W R L and Segall B 1992, *Mater. Res. Soc. Proc.* Vol. 242, p 367

Lambrecht W R L and Segall B 1993a, in *Properties of the Group-III Nitrides*, ed. Edgar J H, Data Review Series of the Electronic Materials Information Service (EMIS) of the British Institution of Electrical Engineers (IEE), (IEE, Stevenage Herts, England), to be published

Lambrecht W R L , Segall B , Suttrop W , Yonagathan M, Devaty R P, Choyke W J, Edmond J A, Powell A J , and Alouani M 1993b, *Appl. Phys. Lett.* **63** 2747

Lambrecht W R L and Segall B 1993c, *Phys. Rev. B* **47** 9289

Safaraliev G K , Tairov Yu M, and Tsvetkov V F 1991, *Sov. Phys. Semicond.* **25** 865

Suttrop W, Yonagathan M, Devaty R P, Choyke W J, Edmond J A, Powell A J, Lambrecht W R L, Segall B, and Alouani M 1993, this Conf. Proc.

ORIGINAL PAGE IS
OF POOR QUALITY

CAN POLAR INTERFACE ENERGIES BE CALCULATED BY MEANS OF SUPERCELLS?

W. R. L. LAMBRECHT, C. AMADOR and B. SEGALL
Department of Physics, Case Western Reserve University, Cleveland, OH 44106-7079

ORIGINAL PAGE IS OF POOR QUALITY

PRECEDING PAGE BLANK NOT FILMED

ABSTRACT

Two problems associated with the calculation of polar interface energies in semiconductors or insulators are discussed: (1) the stoichiometry of the associated interface region, and (2) the impossibility of constructing a supercell with two equivalent interfaces in certain cases. An approach for calculating the energy of a single interface is introduced. It utilizes local quantities obtained from supercell calcualtions and the electrostatic energy of the isolated single interface. Results are presented for GaAs inversion domain boundaries and NaCl antiphase boundaries. The problem associated with charge transfer between two different interfaces is discussed.

INTRODUCTION

The most frequently used approach to describe defects in solids and/or interfaces between two solids employs supercells. In this method, one studies a model system with artificially introduced periodic boundary conditions. This allows one to use the standard band-structure methods because the electronic structure problem is reduced to that of a crystal with a large unit cell. Although in this way one introduces spurious defect interaction effects, these can be minimized by choosing sufficiently large supercells. This approach is very useful in practice, because total energy differences tend to be well described with fairly small supercells. Typically, a few layers of each material are sufficient for an interface calculation.

Nevertheless, there are certain interface problems which cannot be addressed by means of this approach. The reason for this is that in a supercell description of an interface system, there are, in general, two *different* interfaces. One can thus not obtain the interface energy as the difference between the supercell and the corresponding bulk energy, but only the sum of the two different interface energies. One can, of course, always calculate the electronic structure and even local changes in total energy due to relaxation, but not the *absolute value* of the interface energy. In the present paper, we present a new approach, which allows us to solve this problem.

Below, we first discuss the definition of the interface energy in the Gibbs sense [1] and show that there is a problem with polar interfaces related to the definition of the stoichiometry and the choice of the interface region. By polar interfaces are meant interfaces along crystallographic planes which are not neutral in the bulk solid because they do not contain an equal number of cations and anions.

Next, we introduce our new approach, which is based on the use of a cellular band-structure method such as the linear-muffin-tin orbital (LMTO) method in the atomic-sphere-approximation (ASA) [2]. In this sense, the method is closely related to multiple scattering techniques. The division of the total energy in local intra-cellular terms and inter-cellular interactions is what allows us to calculate the energy differences required for a single (i.e. isolated) interface between two *semi* infinite solids. The underlying framework of our approach is the density functional theory in the local density approximation [3].

In the present approach, we use the local quantities obtained from a supercell calculation. This approach is not completely self-consistent because the local quantities near each interface in a supercell may not be the same as near an isolated interface. However, using a trial charge density is in principle justified by the variational principle of the density functional theory [3]. We note, that, a completely self-consistent treatment requires a Green's function method. The present work, in fact, is a step in the development of such a Green's function method [4, 5].

The main example for which we will investigate the problem is that of inversion domain

Ref. 7

boundaries (IDB) [6, 7] in GaAs. These are boundaries between two regions of the zincblende crystal with inverted cation and anion positions. As a result, there are under- and oversatisfied bonds (in the sense of the octet rule) and a large charge transfer can occur between two boundaries of opposite type in the same system. We will show that this imposes a serious limitation on the accuracy of the supercell approach to interface energies, even when our new approach is applied. On the other hand, it allows us to investigate the qualtitative effects of the charge state of the interface.

THEORY

The Gibbs definition [1] of the interface energy γ' at zero temperature and pressure is

$$\gamma' \Omega = E' - \sum_{\alpha} N'_{\alpha} \mu_{\alpha}. \tag{1}$$

where, Ω is the cross-sectional area of the chosen interface region that extends into the bulk on either side of the interface; E' is the excess total energy in the interface region (that is, the total energy minus the bulk energy corresponding to the total number of stoichiometric bulk unit cells contained in the interface region); N'_{α} similarly is the *excess* number of atoms of species α; and μ_{α} is their chemical potential, i.e. the energy per atom of species α. For a macroscopic system, the resulting interface energy γ' is independent of the choice of the interface region, because a homogeneous energy density can be assumed to exist in the bulk regions. The bulk energy of the A and B parts of the interface region with volumes $V_{A(B)}$ are then written as $u_A V_A + u_B V_B$ with $u_{A(B)}$ the respective energy densities. This, however, cannot be done at an atomic scale. Clearly, for a polar interface, γ' will be different when we terminate the interface region with a cation or with an anion layer. In order to maintain the uniqueness of the interface energy, Chetty and Martin [8] recently proposed to define interface regions bounded by symmetry planes of the crystal structure. This leads to a well defined counting of the atoms (in other words a definite stoichiometry of the interface) and the corresponding energy associated with them. We note that for a general crystal structure there might not be any symmetry planes and this proposed rule, which is in any case only a convention, cannot be applied. This shows that at an atomic scale, the interface energy depends crucially on the choice of the interface region.

From the above, we see that the interface energy depends on the chemical potentials of the excess atoms. For a binary compound, the stoichiometry condition in the bulk, $\mu_A + \mu_B = \mu_A^0 + \mu_B^0 + \Delta H_f$, along with the assumption of thermodynamic equilibrium between bulk and interface regions allows us to limit the range in which the chemical potentials can vary [9]. Here, the superscript ^{0} indicates the value of the chemical potential in the standard state at zero temperature and pressure, i.e. the bulk solids A and B, and ΔH_f is the energy of formation of the AB compound. The interface energy only depends on the difference $\Delta\mu = \mu_A - \mu_B$ which is limited to the range

$$\Delta\mu^0 + \Delta H_f \leq \Delta\mu \leq \Delta\mu^0 - \Delta H_f. \tag{2}$$

The lower (upper) limit is the A (B) rich limit in which the system is in thermodynamic equilibrium with a bulk A (B) reservoir.

METHOD

As already mentioned in the introduction, the method we propose here is based on the separation of the total energy in intra- and inter-cellular interactions

$$E_{tot} = \sum_{\alpha} E_{\alpha} + \frac{1}{2} \sum_{\alpha,\alpha'} E_{\alpha,\alpha'}, \tag{3}$$

where E_s is the density functional total energy contribution associated with the charge density in the cell s

$$E_s = \int^{\epsilon_F} N_s(\epsilon)\,\epsilon\,d\epsilon - \int_s\int_s \frac{\rho_s(\mathbf{r})\rho_s(\mathbf{r}')}{|\mathbf{r}-\mathbf{r}'|}\,d^3r d^3r' + \int_s \left[\epsilon_{xc}[\rho_s(\mathbf{r})] - \mu_{xc}[\rho_s(\mathbf{r})]\right]\rho_s(\mathbf{r})\,d^3r, \quad (1)$$

where $N_s(\epsilon)$ is the local density of states, $\rho_s(\mathbf{r})$ is the local charge density, ϵ_{xc} and μ_{xc} are the exchange-correlation energy and potential. Atomic units with energies in Rydberg are used. The interaction between the cells, $E_{s,s'}$, is in general a multipole interaction lattice summation. In the ASA, the latter reduces to a point charge interaction term, i.e. a Madelung sum, because of the spherical symmetry of the charge density assumed inside the spheres.

The latter can be evaluated for the geometry of a single interface between two semi-infinite solids by means of a layer-by-layer summation. Using a two-dimensional (2D) Fourier expansion, the potential of the point charges at sites $\mathbf{r}_i$ in a plane, at point $(\mathbf{r}, z)$ with $\mathbf{r}$ the component in the plane and z the component perpendicular to the plane, is given by

$$V(\mathbf{r},z) = \sum_i{}' \frac{2}{[|\mathbf{r}-\mathbf{r}_i|^2 + z^2]^{1/2}} = \frac{2}{\Omega_2}\sum_{\mathbf{G}\neq 0} \exp[i\mathbf{G}\cdot\mathbf{r}]\frac{\exp[-zG]}{G} + 1\cdot|z| \quad (2)$$

One sees that the $\mathbf{G} \neq 0$ contribution to the electrostatic potential decays exponentially away from the plane with a decay length equal to the smallest non-zero reciprocal lattice vector, i.e. within a distance comparable to the lattice spacing of the charges in the plane. For the potential on the plane itself, a 2D version of the Ewald procedure is used, following Tosi [10]. The $\mathbf{G} = 0$ term diverges for each charged plane separately, but this is associated to the choice of the boundary conditions. It represents the potential of a uniform sheet of charge, which has a change in the electrostatic field component normal to the plane $\Delta E_z = 8\pi\sigma$ where σ is the surface charge density. The one-dimensional Poisson equation describing the potential of a set of uniform charged sheets can be solved easily with the appropriate boundary condition that the potential and the electric field averaged over a period (unit cell) in the asymptotic periodic region on one side of the interface should vanish. On the other side of the interface, the average electric field far away should likewise vanish, which requires the interface region to be neutral, but the average potential may be shifted by a constant dipole term. We see that if we had an interface with a net charge, the potential would diverge linearly and thus the energy associated with it. In practice, charged interfaces in insulators or semiconductors can exist only because they are compensated by space charge layer. The latter result from the ionization of impurity levels and for a typical doping level can extend over several 1000 Å. The space charge region, which contains a total charge equal in magnitude and opposite in sign to that of the interface region, introduces a boundary condition for the electrostatic potential and its slope at its boundary with the interface region.

The charges in the semi-infinite model are obtained from a supercell calculation for the atoms close to the interface and from a bulk calculation for the atoms which are farther away from the interface. We use equivalent k-point sets for the supercells and the bulk calculation to optimize the accuracy. When the charges thus obtained lead to a charged interface region we add a compensating charged sheet so as to avoid the divergence of the total energy. The latter can either be put at the last interface layer or at the first bulk-like layer. This compensation charge is, at present somewhat arbitrary and we will investigate its effects on the results. In a self-consistent Green's function calculation of the interface this arbitrariness is resolved. Normally, one will determine the interface region's potential so that charge neutrality is obtained. For a charged interface region, the net charge inside the interface region is determined by the local position of the Fermi level. The latter is pinned in the bulk by the impurity levels which give rise to the space charge region. The resulting electrostatic potentials and their slopes at the boundary between the interface region and the space charge region must match. For a given impurity level and spatial distribution in the space charge region, there is only one net charge for which this can be achieved self-consistently. The interface energy thus will depend on the charge state which in turn is determined by the impurity distribution.

ORIGINAL PAGE IS
OF POOR QUALITY

III. RESULTS

As a first test of the new approach for calculating interface energies, we consider the non-polar {110} interfaces. In that case, we can straightforwardly compare the results of the supercell energy difference approach and the new approach. The results are shown in Table I. This table shows that the two methods are in agreement for a supercell size of at least four layers in each domain. The decomposition into the intra-sphere and intersphere terms of Eq. (3) is also indicated in the table. Similar results are obtained for NaCl, (given in Table II), a case where one expects a

Table I. Interface energies of the {110} GaAs IDB in meV/Å^2.

cell	supercell method			new approach		
	$\sum E_s$	$\sum E_{s,s'}$	total	$\sum E_s$	$\sum E_{s,s'}$	total
3 + 3	47.5	-10.9	36.6	41.2	-1.0	40.2
4 + 4	44.6	-11.0	33.6	44.6	-11.2	33.4
5 + 5	44.7	-10.2	34.5	46.6	-12.5	34.1

larger effect of the re-calculation of the electrostatic terms on the interface energy. The relative change is indeed somewhat larger, although, surprisingly the anti phase boundary in NaCl costs less energy than that of the inversion domain boundary in GaAs.

Table II: Interface energies of NaCl {110} antiphase boundary in meV/Å^2.

cell	supercell method			new approach		
	$\sum E_s$	$\sum E_{s,s'}$	total	$\sum E_s$	$\sum E_{s,s'}$	total
3 + 3	10.4	-7.2	3.2	9.4	-7.7	1.7
5 + 5	11.4	-8.2	3.2	10.6	-8.0	2.6

Next, we consider the polar {001} interfaces. Because of the fourfold rotary reflection symmetry in the zincblende structure, one can still construct a supercell with two equivalent interfaces in this case. The latter is, however, not stoichiometric. In this case, the interface energy depends on the choice of the chemical potentials. We give the results for the Ga and As-rich limits [11]. The supercell results are given in Table III. On the other hand, we can also use a non-symmetrical supercell, i.e. a cell with two different interfaces, one Ga-Ga and one As-As IDB. The latter is a stoichiometric. Because our cells containing two interfaces of the same type contained two domains of different size one can use the local quantities of either one of those domains to transfer them to the semi-infinite model. The various choices and their associated energies are listed in Table IV. Finally, in that table we indicate (in parentheses) the effect of using two different charge compensation methods. The first value is obtained putting the compensating charge on the first bulk-like layer, the second on the last interface layer.

We note that the Ga boundary energy comes mostly from the intra-sphere term and is thus relatively insensitive to this choice, while the As-boundary has a large electrostatic contribution

Table III: Interface energies obtained with the supercell energy difference method for GaAs {001} IDBs in meV/Å^2.

cell formula	boundary	Ga rich	As rich
$(Ga_3As_2)(Ga_4As_3)$	Ga-Ga	26	69
$(Ga_2As_1)(Ga_1As_4)$	As-As	91	49

Table IV: Interface energies obtained with the new approach for {001} GaAs IDBs in meV/Å². Parentheses indicate alternate compensation method.

cell formula	part of cell used	boundary	Ga rich	As rich
$(Ga_3As_2)(Ga_4As_3)$	right	Ga-Ga	35 (35)	77 (77)
$(Ga_3As_2)(Ga_4As_3)$	left	Ga-Ga	26	69
$(GaAs)_5(GaAs)_3$	near Ga-Ga	Ga-Ga	6 (6)	48 (48)
$(GaAs)_5(GaAs)_5$	near Ga Ga	Ga-Ga	12 (12)	54 (54)
$(Ga_2As_3)(Ga_3As_4)$	right	As-As	85 (96)	42 (54)
$(Ga_2As_3)(Ga_3As_4)$	left	As-As	94	52
$(GaAs)_5(GaAs)_3$	near As-As	As-As	103 (93)	61 (51)
$(GaAs)_5(GaAs)_5$	near As-As	As-As	92 (80)	50 (38)

and is thus relatively sensitive to this choice. Secondly, we note that the boundary energies extracted from the symmetrical cells are in good agreement with the supercell energy difference results. The As-IDB energy obtained from the non-symmetrical cell is also in fair agreement with these results. The Ga-IDB, however, turns out to have a much lower energy in the supercell which contains two different interfaces. This is a manifestation of its different charge state. We find that there is considerable electron transfer from the As-IDB to the Ga-IDB in this cell which increases as the cell size decreases. The increased number of electrons in the Ga spheres leads apparently to a lower energy. This may be associated with the fact that the Ga-Ga bonding states introduced near the valence band maximum become filled with electrons. Elsewhere, we have discussed the interaction of these interfaces in detail [7]. The electrons are here provided by the n-type or donor-like As-IDB, but similar results would presumably hold for a Ga-IDB interacting with any other n-type dopant.

Table V: Interface energies of the {111} GaAs IDB in meV/Å². Parentheses indicate alternate compensation method.

boundary	Ga-rich	As-rich
Ga-Ga	-38 (-40)	-13 (-15)
As-As	73 (71)	48 (46)

Finally, we considered the {111} interface by means of a $(GaAs)_3(GaAs)_3$ cell. In this case, the usual supercell energy difference approach is not at all applicable because of the absence of any symmetry related to the {111} planes. This can also be seen by considering the alternation of long and short interplanar distances in the (111) direction. The net stoichiometry of this interface, according to Chetty and Martin's [8] counting procedure is an excess of $\frac{1}{2}$ Ga or $\frac{1}{2}$ As. The boundaries considered have only one wrong bond per interface unit area. As a result they have a smaller average energy (obtained from the supercell energy difference to be 30 meV/Å²) than the {110} and {001} interfaces. The individual energies obtained are given in Table V.

That the energy of the Ga IDB here becomes negative, is probably an artifact associated with the small size of the supercell and the resulting large charge transfer. This does not indicate that these boundaries should form spontaneously. The high energy of the As IDB, whose presence is required to produce this result, more than compensates the negative energy. The low energy of the {111} Ga IDB when negatively charged is consistent with the results for the {001} interface.

ORIGINAL PAGE IS OF POOR QUALITY

CONCLUSIONS

We have presented a new method for extracting interface energies from the results of supercell calculations applicable to polar interfaces and to cases, where a supercell containing two equivalent interfaces cannot be constructed. Good agreement is obtained with the usual supercell energy difference approach in cases where the latter is applicable. When large charge transfers occur, as is the case in the example presented here of polar GaAs IDBs, considerable uncertainty is associated with the way in which this charge is compensated. This is a reflection of the non-self-consistency of the procedure. A Green's function method will be required to address this problem in a completely satisfactory manner. The development of such a method is presently in progress. *From our present calcualtions, we found that charged interfaces may have a lower energy than neutral ones if appropriately compensated by a charge distribution elsewhere in the system.*

This work was supported by D.A.R.P.A.-O.N.R. and the N.A.S.A. Lewis Research Center.

REFERENCES

1. J. W. Gibbs *Trans. Conn. Acad.*, III, 108 (1876); *ibid.* 343 (1878), in *The Collected Works of J. Willard Gibbs*, Vol. I, (Yale University Press, New Haven 1948). See particularly p. 219 and following.

2. O. K. Andersen, *Phys. Rev. B* 12, 3060 (1975); O. K. Andersen, O. Jepsen, and M. Šob, in *Electronic Band Structure and its Applications*, edited by M. Yussouff, (Springer, Heidelberg, 1987).

3. P. Hohenberg and W. Kohn, *Phys. Rev.* 136, B864 (1964); W. Kohn and L. J. Sham, *ibid.* 140, A1133 (1965).

4. W. R. L. Lambrecht and O. K. Andersen, *Surf. Sci.* 178, 256 (1986); and unpublished.

5. H. L. Skriver and N. M. Rosengaard, *Phys. Rev. B* 43, 9538 (1991).

6. W. R. L. Lambrecht, C. H. Lee, M. Methfessel, M. van Schilfgaarde, C. Amador, and B. Segall, *in Defects in Materials*, edited by P. D. Bristowe, J. E. Epperson, J. E. Griffith, and Z. Liliental-Weber, Mat. Res. Soc. Symp. Proc., Vol. 209, (MRS, Pittsburgh, 1991), p. 667.

7. W. R. L. Lambrecht, C. Amador, and B. Segall, submitted to *Phys. Rev. Lett.* (1991)

8. N. Chetty and R. M. Martin, *Phys. Rev. B* 44, 5568 (1991).

9. G. X. Qian, R. M. Martin, and D. J. Chadi, *Phys. Rev. B* 38, 7649 (1989).

10. M. P. Tosi, in *Solid State Physics, Advances in Research and Applications*, edited by F. Seitz and D. Turnbull, (Academic, New York 1964), Vol. 16, p. 1. (See particularly the Appendices)

11. The Ga fcc and As sc energies were used as "standard" chemical potentials. With the total energy of GaAs they give a ΔH_f of -0.71 eV/cell, which is in good agreement with the experimental value of -0.74 eV/cell.